JOURNAL OF GEOPHYSICAL RESEARCH, VOL. 95, NO. D7, PAGES 9983–10,004, JUNE 20, 1990

Potential Evapotranspiration and the Likelihood of Future Drought

D. RIND,[1] R. GOLDBERG,[2] J. HANSEN,[1] C. ROSENZWEIG,[2] AND R. RUEDY[3]

The likelihood of future drought is studied on the basis of two drought indices calculated from the Goddard Institute for Space Studies general circulation model (GISS GCM) transient and doubled CO_2 climate changes. We use the Palmer drought severity index (PDSI) and a new supply-demand index (SDDI), the latter being the difference between the precipitation and potential evapotranspiration E_P, i.e., the difference between atmospheric supply of and demand for moisture. Both indices show increasing drought for the United States during the next century, with effects becoming apparent in the 1990s. If greenhouse gas emissions continue to increase rapidly, the model results suggest that severe drought (5% frequency today) will occur about 50% of the time by the 2050s. The results are driven by the large increase in E_P, associated with the simulated climate warming. E_P increases most where the temperature is highest, at low to mid-latitudes, while precipitation increases most where the air is coolest and easiest to saturate by the additional moisture, at higher latitudes. Thus atmospheric demand becomes greater than supply for most of the globe by the latter half of next century. We show that large E_P changes can lead to soil moisture deficits, as in the PDSI hydrologic budget, and vegetation desiccation, as is implied by vegetation and climate models. We suggest that drought intensification has been understated in most GCM simulations, including the GISS GCM, because of their lack of realistic land surface models. Paleoclimate analogues in the Mesozoic and Cenozoic are reviewed which imply that arid conditions can result from either increased temperatures or decreased precipitation, consistent with our use of the SDDI. The results depend primarily on the temperature increase, in particular the model sensitivity of 4°C warming for doubled CO_2. Global precipitation cannot keep pace with increased demand over land because the land surface warms more than the ocean surface; this effect, along with greater atmospheric opacity, reduces low level gradients and evaporation from the ocean. If the forecast temperature changes come to pass, these conclusions suggest that drought conditions will increase dramatically.

1. INTRODUCTION

The anticipated increase in temperature associated with accumulating greenhouse gases has led to the concern that future water availability might be threatened [*Smith and Tirpak*, 1989], as warmer temperatures will likely lead to increased evaporation. Several approaches have been employed to evaluate this possibility. *Stockton and Boggess* [1979] used an empirical relationship derived by *Langbein* [1949] to assess the effect of a 2°C temperature increase and a 10% precipitation decrease (values consistent with some general circulation model (GCM) projections). They found on average a 50% reduction in water supply for seven western United States water regions. *Karl and Riebsame* [1989] criticized the Langbein relationship and concluded from the climate record over the United States that the influence of temperature on water availability is much more muted. *Revelle and Waggoner* [1983] correlated past temperature changes with river flows of the Colorado River, and with a 2°C increase they deduced a 30% decrease in runoff.

There are serious difficulties in using the observational record for this type of analysis. The temperature changes in the historical past are very small compared with projections; the average warming used in the *Karl and Riebsame* [1989] study was only 1/10 that being projected for doubled CO_2, an important consideration given that the water-holding capacity of the atmosphere and hence evaporation varies strongly with temperature. In addition, there is a built-in bias in empirical studies, for warmer summers are commonly associated with reduced precipitation, both driven by the presence of a large mid-tropospheric ridge. In the doubled CO_2 climate, the warming is widespread, driven by the global energy balance, and past correlations may no longer hold.

Alternatively, one could use the GCM model output itself to estimate the likelihood of water availability changes. The problem with this approach is that although some models predict summer drying [*Manabe and Wetherald*, 1987], precipitation changes are not consistent from model to model [*Schlesinger and Mitchell*, 1987] or even in varied experiments with the same model [*Rind*, 1988*a*], and thus neither are the resulting changes in soil moisture [*Kellogg and Zhao*, 1988; *Zhao and Kellogg*, 1988].

Using the GCM soil moisture changes to evaluate the likelihood of drying has built-in limitations. For one thing, in several of the models, summer soil moisture decreases to very small values in the control run [*Kellogg and Zhao*, 1988]. Not much drying in absolute terms is possible under such circumstances, since soil moisture values cannot drop below zero. Furthermore, the dry soil limits evaporation efficiency (β) in GCMs in an unrealistic manner. This point, which has been largely overlooked, will be discussed further in section 3.

The models are in greater accord on the temperature change projections, with all models showing warming of some 2°–5°C over the United States, varying somewhat with season. Higher temperatures increase the atmospheric water-holding capacity and thus the ability of the atmosphere to draw moisture from the surface. Given the large increase in atmospheric water-holding capacity associated with the projected temperature increases, of the order of 33%, it is somewhat surprising that the GCMs are not in more obvious agreement as to projections of future soil moisture condi-

[1]Institute for Space Studies, Goddard Space Flight Center, New York.
[2]Center for the Study of Global Habitability, Columbia University, New York.
[3]Central Sigma Data Services Corporation, New York.

Paper number 90JD00026.
0148-0227/90/90JD-00026$05.00

tions. We explore reasons why the large temperature increases do not have greater impact on the GISS (and other) GCM soil moisture projections.

In this paper, we reexamine the question of the likelihood of future droughts. We consider "drought" as the condition resulting from an excess of the atmosphere's demand for moisture over its supply. We attempt to validate this definition by discussing the importance of potential evapotranspiration E_P in considerations of drought, and we show that increases in $E_P - P$ (precipitation) can lead to decreased soil moisture and/or increased vegetative stress, neither of which is properly assessed in GCMs owing to their crude treatment of ground hydrology.

We then develop a new drought index, constructed from $E_P - P$, and compare it with the well-known Palmer drought severity index (PDSI). We use both indices to evaluate the likelihood of future drought, given the climate change projections generated by the Goddard Institute for Space Studies (GISS) GCM. We show that the two indices give similar results, both suggesting substantial increases in future drought; the projection is thus not the result of one particular index formulation.

In the discussion section we examine how the uncertainties in future climate projections impact the likelihood of future drought. We consider the issue of desiccated vegetation more closely by assessing the possible impact of these drought projections on vegetation biomass and type. We then discuss why large E_P increases will likely lead to increasing desertification regardless of whether the initial response of the system is on the hydrologic or vegetative aspect. Finally, we attempt to validate the general conclusion from paleoclimatic evidence. The results suggest that the climate warming as currently envisioned could severely increase drought conditions.

2. The Importance of Potential Evapotranspiration

Potential evapotranspiration E_P is the atmospheric demand for water. This moisture demand is felt directly by free water surfaces, such as lakes or reservoirs, where E_P is equal to the actual evapotranspiration (ET). E_P is also approximately equal to transpiration when a plant is consuming water at a rate which gives the optimum plant development, and thus for active, non-water-stressed plants, E_P is translated into ET with near-100% efficiency; for example, *Penman* [1948] estimated that the ratio β between actual and potential ET rates for southern England ranged from 0.6 in winter to 0.8 in summer. Estimates of E_P over vegetated surfaces and free water bodies are generally about 3–5 mm d^{-1} [e.g., *Thornthwaite*, 1948].

Free water and vegetated surfaces account for a substantial portion of total ET, especially during the growing season. Transpiration alone accounts for the loss of about 70% of the water which falls on the continental United States [*Yao*, 1981], and about 85% of total ET in the Amazon rain forest [*Shuttleworth et al.*, 1984]. *Kramer* [1983] estimates that evaporation from soil is only about 10% of the total water loss in forests, and about 25% in meadows.

Plants limit their water loss below the potential rate chiefly by closing their stomata, small openings on leaf surfaces, under stressed conditions (see, for example, *Kramer* [1983]). Stomata respond to light, humidity, soil moisture, temperature, and wind speed [*Larcher*, 1980], any of which can provide the necessary stress. When the stomata are closed, carbon dioxide is not absorbed, photosynthesis is decreased, and eventually the plant wilts. If this condition lasts sufficiently long, the plants cannot recover.

When stomata are closed, water loss is limited, which reduces the value of β. On the biome level, therefore, low values of β in temperate areas imply stressed vegetation. In arid areas, on the other hand, where plants have adjusted to dry conditions, β is normally small, which limits photosynthesis and biomass, resulting in sparse vegetation cover. Values of β for land surfaces in deserts are of the order of 0.2 (D. Hillel, personal communication, 1989).

It is this reasoning that led *Thornthwaite* [1948, p. 56] to emphasize the importance of E_P in assessing moisture availability.

> The vegetation of the desert is sparse and uses little water because water is deficient. If more water were available, the vegetation would be less sparse and would use more water. There is a distinction then, between the amount of water that actually transpires and evaporates and that which would transpire and evaporate if it were available.

Since E_P represents the value of ET which would prevail under optimal growing conditions, *Thornthwaite* [1948, p. 75] concludes,

> It is now apparent that the actual evaporation and transpiration from the soil is not what must be compared with precipitation in order to obtain a moisture index, but, rather, the potential evapotranspiration. Where precipitation is exactly the same as potential evapotranspiration all the time and water is available just as needed, there is neither water deficiency nor water excess, and the climate is neither moist nor dry. As water deficiency becomes larger with respect to potential evapotranspiration, the climate becomes arid; as water surplus becomes larger, the climate becomes more humid.

The importance of potential evapotranspiration, as opposed to actual evapotranspiration, in determining the vegetation response to climate on the biome level has generally been recognized in climate classification schemes. For example, the well-known *Köppen* [1936] classification scheme defines a dry climate (Köppen's "B" climate) as one in which potential evapotranspiration exceeds precipitation; included in this category are deserts, steppes, and prairies. The same general procedure applies in numerous other classification schemes [*Prentice*, 1990]

The above discussion reveals that the use of GCM soil moisture changes, which are approximated by changes in precipitation minus evaporation (plus runoff), may not provide an adequate indication of future drought conditions. Analysis which focuses on the changes in precipitation and potential evapotranspiration could be more relevant. The differences between these two approaches will become evident in the next section when we discuss the hydrology schemes currently used in GCMs.

3. Potential Evapotranspiration in GCMs and Implications for Soil Moisture and Vegetation Changes

In the GISS GCM, potential evapotranspiration is parameterized with an aerodynamic formulation in terms of the difference between the (saturated) ground level specific humidity q_G, the atmospheric specific humidity q_S (at ap-

TABLE 1. Summer Hydrologic Budgets Averaged Over the United States for the Current Climate and the 2050s, in the GCM and PDSI

	GISS GCM		PDSI	
	Current	Δ2050s	Current	Δ2050s
Soil moisture, mm	89	2.19	150	−22.3
Precipitation, mm d^{-1}	3.05	0.43	3.05	0.40
Evaporation, mm d^{-1}	3.52	0.28	3.32	0.68
Runoff, mm d^{-1}	0.48	0.14	0.47	−0.14
Water loss, mm d^{-1}	0.92	−0.01	0.89	0.18
β	0.23	−0.01	0.89	0
E_P, mm d^{-1}	33.5	10	3.8	0.97
Field capacity, mm	366		202	

Here β is the efficiency factor and E_P is potential evapotranspiration.

proximately 30 m height), the surface wind speed V, and the local turbulent transfer coefficient C_Q,

$$E_P = C_Q V(q_G - q_S) \quad (1)$$

Actual ET is parameterized as the product of E_P and the efficiency factor β,

$$ET = \beta E_P \quad (2)$$

For actual land surface conditions, β depends on soil type, ground wetness, and plant properties [*Baier et al.*, 1972; *Hillel*, 1971]. In the GISS GCM we take β to be the fractional wetness of the first layer of the ground (10 cm) or, during the growing season, the sum of the two ground layers (4.1 m) [*Hansen et al.*, 1983]. This results in less evaporation as the ground dries. Other GCMs use a similar type of formulation [*Carson*, 1982], although the depth over which β or its equivalent is calculated varies; in the GFDL model, a depth of 1 m is used [*Manabe*, 1969]. The relationship of β to ground wetness in GCMs thus varies in a linear fashion, and at least once available soil moisture drops below certain levels, this is in accordance with some observations [e.g., *Rosenthal et al.*, 1985; *Gollan et al.*, 1986].

The United States hydrologic balance for the GISS GCM during summer for the control run climate is shown in Table 1. Note in particular the low value of β, approximately 20%. This small value of β is unrealistic for the current climate, as observations suggest a value of β between 0.6 and 0.9 [*Hillel*, 1980]. Given that plants grow optimally with a value of β close to 1, the GISS model is effectively assuming that plants are growing poorly or are sparse (approximating desert conditions); the PDSI has values of 0.2 for states without much vegetation, such as Arizona. Furthermore, the E_P values obtained are very large. Similar large E_P values are obtained in the Geophysical Fluid Dynamics Laboratory (GFDL) model [*Delworth and Manabe*, 1988]. Low values of β characterize many areas in the GCM (Figure 1).

The problem arises because the GISS GCM, as is the case with the other GCMs which have been used for doubled CO_2 climate change projections, does not actually contain a vegetated surface, i.e., a canopy. Real world vegetation is usually transpiring (has available water); thus available energy is used for transpiration, and the canopy surface temperature does not get very warm. In contrast, the land surfaces in GCMs have limited water availability and experience strong temperature increases during sunlit portions of the day. As the ground temperature rises, large gradients in $T_G - T_S$ become established, leading to large values of $q_G - q_S$, and large drag coefficients. This increases the E_P values, dries out the soil, and lowers the value of β [e.g., *Sud and Fennessy*, 1982]. The low values of β keep ET rates at reasonable levels, given the large E_P values. Over water

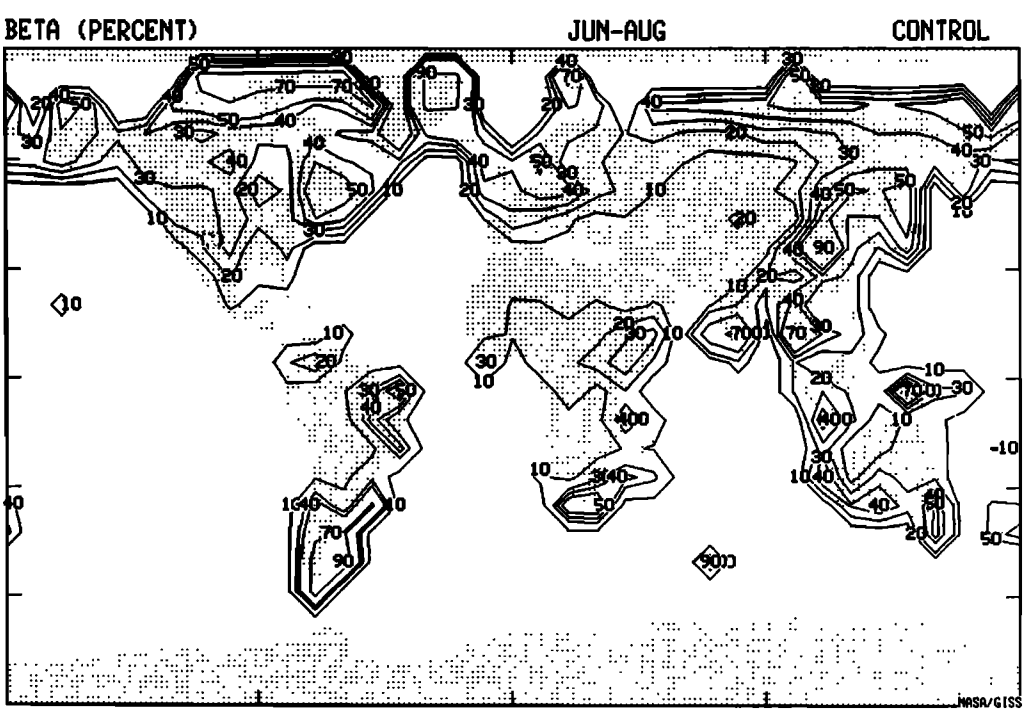

Fig. 1. Average value of β in the GISS GCM during June–August for the control run (current climate).

surfaces, where $\beta = 1$, $E_P = E$, and the GCM rates are reasonable (global average evaporation for the GISS current climate simulation is 3.1 mm d^{-1}).

What effect does this deficiency have on the GCM estimate of soil moisture change? Table 1 includes the hydrologic changes over the contiguous United States averaged for summers in the 2050s, using the climate change estimates produced by the GISS GCM with trace gas increases assumed in GISS scenario A [*Hansen et al.*, 1988]. The large temperature increase (of 4.2°C) results in a E_P increase of about 30% as Q_G and Q_S go up accordingly. However, the small value of β limits the actual ET change to less than 10%, as is shown schematically in alternative A below. Since the ET increase does not exceed the precipitation increase, soil moisture does not change appreciably.

(A) $ET = \beta_{small} E_P$ (B) $ET = \beta_{large} E_P$ (C) $ET = \beta E_P$

With larger (and more realistic) values of β, the response to large E_P increases is to produce appreciable evaporation increases, reducing soil moisture (as we show below when discussing the PDSI results). This is illustrated in alternative B. Then with reduced soil moisture, vegetation desiccation is likely to arise on the short time scale, and, on the longer time scale there is likely to be a change to sparser vegetation. This would lead to a decrease in the efficiency factor β, which might offset the E_P increase, resulting in little ET change (alternative C) but reduced biomass.

At this stage of GCM development we cannot determine which of the three alternative outcomes for ET and thus soil moisture will arise in any particular location. What they all have in common is the driving force, the E_P increase. In this paper, then, we define drought as that condition which arises from an excess of E_P over precipitation, which could result in either increased ET (soil moisture decrease) or decreased β (biomass decrease). In the following study we make use of an index derived directly from precipitation and potential evapotranspiration to evaluate the likelihood of future droughts.

4. Drought Indices

4.1. *The "Supply-Demand" Drought Index*

Given the GCM magnitude of potential evapotranspiration shown in Table 1, we cannot use the simple rule that a dry climate is one in which potential evapotranspiration exceeds precipitation ($E_P > P$), either for the current climate or for climate change projections. However, we can still use the change in $P - E_P$ to indicate changes in the tendency toward drying conditions. As precipitation is the atmospheric supply of water and E_P is the atmospheric demand, we use the change in $P - E_P$, normalized to account for current variability, to generate a drought index referred to as the "supply-demand" drought index, or SDDI. In a form analogous to that of the Palmer drought severity index (PDSI), we define the difference between the actual $P - E_P$ and the model's climatological average for each grid box as

$$d_{SDDI} = P - E_P - (P - E_P)_{clim} \quad (3)$$

TABLE 2. Comparison of SDDI and PDSI Absolute Index Values for a Succession of Months With 1σ Decrease in $P - E_P$

	Month						
	1	2	3	4	5	6	7
Change in $P - E_P$	-1σ	-1σ	-1σ	-1σ	-1σ	-1σ	$+4.2\sigma$
SDDI	−1.0	−1.9	−2.7	−3.4	−4.1	−4.7	0.0
PDSI	−0.5	−1.0	−1.7	−2.2	−2.7	−3.1	−0.2

The result of a 4.2σ increase is shown for the seventh month.

and the "moisture anomaly index" Z as

$$Z_{SDDI} = d/\sigma \quad (4)$$

where σ is the interannual standard deviation in the monthly $P - E_P$ from the control run. The moisture anomaly index Z thus increases by 1 whenever the difference between P and E_P for the current month is 1 standard deviation greater than the climatological control run difference.

As drought and soil moisture deficit are cumulative phenomena, the drought index for the current month, $Y(i)$, is related to the index from the previous month, $Y(i-1)$, as in the PDSI,

$$Y(i) = 0.897\ Y(i-1) + Z(i) \quad (5)$$

Palmer [1965] found the value 0.897 to maintain the PDSI at a given level from month to month for rates of Z accumulation that maintain a drought of constant severity.

A prime benefit of the SDDI is that it is readily obtained for the entire globe, without the necessity for deriving special coefficients for individual areas, as is the case for the PDSI. Regional hydrological properties are represented in the model physics and the input data sets (i.e., soil and plant characteristics, topography, etc.). All that is needed to generate the SDDI are the monthly average potential evapotranspiration and precipitation values for each grid box.

The SDDI (and PDSI) indices range from negative values for dry months to positive values for wet months. Note that this terminology is utilized relative to local mean conditions, so that, for example, the Sahara normally does not have more negative values than rain forests; at each location the SDDI has a climatological average value of zero by definition (as does the PDSI).

Table 2 shows the values of the SDDI averaged over the United States for a 1σ deficit in $P - E_P$ for 6 months in a row, compared with the PDSI for a similar string of deficit months. The SDDI grows in value somewhat more rapidly than the PDSI; if we had used $Z = d\,(2\sigma)^{-1}$, then the SDDI would have grown somewhat more slowly. In either case, it is clear that the absolute value of the index cannot be used to define the actual drought severity, as it probably should not be for the PDSI [*Alley*, 1984].

In the subsequent analysis we determine for the region in question (either global land areas or the contiguous United States), the range of SDDI and PDSI drought indices in the control run for the 1%, 5%, 16%, and 36% most severe droughts and floods. The same values are then used to determine "droughts" or "floods" for the climate change experiments, and it is these percentages to which we refer in the results section.

4.2. *The Palmer Drought Severity Index*

The PDSI is a widely used index for evaluating drought conditions in the United States. It has been the chief index for comparing historical droughts [e.g., *Karl and Quayle*, 1981; *Karl and Koscielny*, 1982; *Diaz*, 1983; *Hecht*, 1983]. This index has been derived empirically and has many arbitrary rules, some of which will be discussed below, and is thus subject to criticism [e.g., *Alley*, 1984]. Nevertheless, its wide use and continued promulgation by the National Weather Service in evaluating drought-flood conditions make it useful for putting the future climate drought situation in a familiar perspective, and for comparison with the SDDI defined above.

Potential evapotranspiration is a key component in analysis of PDSI [*Palmer*, 1965]. *Karl and Quayle* [1981] analyzed historical monthly data for the United States from 1895 to 1980, and in the process showed the correlation between PDSI values and the "moisture balance" (precipitation minus potential evaportranspiration). Years of extreme drought are equally well characterized by both methods. This fact provides some justification for the formulation of the SDDI (together with its simplicity and the fact that the PDSI parameters are not available globally).

The PDSI uses the *Thornthwaite* [1948] method to calculate E_P. In this approach, the first step is to derive monthly (i) and annual (I) heat indices for each location

$$i = (T/5)^{1.514} \tag{6}$$

$$I = \sum_{1}^{12} i \tag{7}$$

where T is the long-term average temperature in degrees Celsius for the particular month. The unadjusted E_P for a given month is obtained from the formula

$$\text{unadjusted } E_P = 1.6(10 \times T/I)^m \text{ cm} \tag{8}$$

where m depends on I, as

$$m = (6.75 \times 10^{-7})I^3 - (7.71 \times 10^{-5})I^2 + (1.79 \times 10^{-2})I + 0.492 \tag{9}$$

The unadjusted E_P values are then corrected for day length from tables. Note that this formula is applied only for temperatures less than 80°F; for higher temperatures, E_P depends only on temperature, not on I and m.

In addition to the calculation of E_P, the PDSI has a complete water balance model, including runoff, evaporation, and water storage, which differ from the GCM's parameterizations and budgets. The hydrologic budgets derived from the GISS control run temperatures and precipitation are shown in Table 1, along with the PDSI input data for water-holding capacity based on soil type. Note that compared with the GCM, the Palmer budget for the current climate has lower water-holding capacity yet more soil moisture during summer, and a much larger value of β. It also has a much smaller value of E_P. The PDSI water budget values appear to be closer to expectations than those of the GISS model, at least for vegetated surfaces. Notice also that the rates of evaporation, runoff, and soil moisture loss during summer are almost the same as those in the GCM.

To calculate the PDSI, monthly temperatures and precipitation are input to a code for individual states provided by the National Climate Data Center. Model-produced temperatures and precipitation for each state come from the grid box encompassing the major portion of that state (for comparison purposes, the same procedure was followed for the SDDI). From the input climatology, the two Thornthwaite parameters I and m are calculated for the potential evapotranspiration estimate, as are four other coefficients (α, β, γ, δ) which represent the ratios of actual to potential evaporation (E_P), recharge (PR), runoff (PRO) and soil moisture loss (PL), respectively. From these values, the difference d between the actual precipitation P and the "climatically appropriate for existing conditions" precipitation is calculated as

$$d_{\text{PDSI}} = P - (\alpha\, E_P + \beta\, \text{PR} + \gamma\, \text{PRO} - \delta\, \text{PL}) \tag{10}$$

(Note that the coefficient α in PDSI notation is what we have referred to as β, the ratio between actual and potential evaporation, in the discussion above and in Table 1; we will continue to call it β since this is the terminology used in the discipline, except when we are showing PDSI calculations).

The moisture anomaly Z is defined as

$$Z_{\text{PDSI}} = Kd \tag{11}$$

where K is a monthly weighting factor derived from the temperature and hydrologic variables [see *Alley*, 1984]. Finally, the PDSI value for a given month, $X(i)$, is derived from the expression

$$X(i) = 0.897\, X(i-1) + Z(i)/3 \tag{12}$$

Expressions (10) through (12) can be compared with their SDDI equivalent (equations (3)–(5)), which have a similar form. In the following analysis we use both indices to evaluate the likelihood of future drought, given the GISS GCM climate projections.

5. RESULTS

5.1. *SDDI Analysis: Transient Experiment*

Monthly values for the relevant quantities in equations (3)–(5) and the corresponding SDDI values were generated for each grid box of the GISS 8° × 10° resolution model from a 100-year control run with 1958 atmospheric composition [*Hansen et al.*, 1988]. This model has a climate sensitivity of 4.2°C for doubled CO_2. We then calculate what percentage of the time each SDDI value occurs for a given location; the limiting values for the contiguous United States during summer are shown in Table 3, along with the corresponding PDSI value calculated in three different ways (section 6.2, below). In absolute terms, the SDDI values are somewhat more negative or positive for the most extreme events (droughts and floods) than the PDSI values. This makes no difference in the climate change results, which are presented in terms of their frequencies of occurrence in the 100 year control run or in the 1951–1980 climatology.

We use the climate change projections for trace gas growth scenario A in which radiative greenhouse forcing continues to grow at an exponential rate [*Hansen et al.*, 1988]. Plate 1 shows the June–August drought index for four years, 1969, 1999, 2029, and 2059. These can be compared with four other summers during those decades (given by

TABLE 3. Absolute Drought Index Values Which are Exceeded Less Than a Given Percentage of the Time Averaged Over the United States in Summer

	<−1%	<−5%	<−16%	<−36%	>36%	>16%	>5%	>1%
SDDI	−9.6	−6.3	−3.3	−0.9	1.5	3.4	5.3	7.2
PDSI-base	−5.7	−4.0	−2.4	−1.0	0.9	2.3	3.6	4.9
PDSI-ratio	−5.9	−4.1	−2.5	−1.0	1.0	2.5	4.1	6.0
PDSI-actual	−5.6	−4.0	−2.4	−0.9	1.0	2.5	3.9	5.2

Negative values mean dry conditions. See text for PDSI methods.

Hansen et al. [1989]), which show the same basic characteristics. In 1969 there is an equal distribution of wet and dry regions, with extreme occurrences randomly distributed and infrequent. By 1999, very dry conditions occur over some tropical and subtropical land masses. In 2029 the dry regions have expanded, pushing into the United States and increasing in drought intensity, and by 2059, extreme drought covers most mid-latitude locations, including the contiguous United States, while extreme flood conditions are found at the highest latitudes. Note that if trace gas increases are slower than is projected in scenario A or climate sensitivity is less, these effects will be modified accordingly.

The variation of drought occurrence with time is shown in Figure 2 for scenario A averaged over all land points for June–August. Extreme drought conditions occurring less than 1% of the time in the control run increase in frequency during the next century to close to 50% by 2060, the time of global average temperature change of 4.2°C (equivalent to the equilibrium warming for doubled CO_2). We can see from Plate 1 that the increased drought frequency is associated with a northward movement of drought regions as well as an increase in drought severity at particular locations. The regions affected first are those which are warmest to begin with; from the Claussius-Clapeyron equation, an incremental increase in temperature produces a greater increase in atmospheric moisture-holding capacity when the temperature is warmer. The warmest regions thus have a larger change in potential evapotranspiration; *Mather* [1987] found a similar result using the Thornthwaite method for calculating E_P with both GISS and GFDL doubled CO_2 results. In some seasons this is mitigated by the higher latitudes showing greater magnitudes of warming, but in summer the warming is relatively independent of latitude in the GISS GCM.

The frequency of occurrence of the "5% drought" (SDDI values which were exceeded only 5% of the time in the control run) in the United States for the summers of the 1990s is shown in the top left-hand portion of Plate 2. Droughts are already on the increase by this time, with higher frequency of the 5% drought occurring in some southeastern and western portions of the United States. This regional distinction is associated with a changed circulation due to increasing land-ocean contrast. Because the ocean warms more slowly, high-pressure systems over the ocean are intensified, leading to greater southerly flow of warm air along the gulf coastal states, and greaterly northerly flow of dry air in the west. Similar processes can be seen elsewhere (Plate 1); for example, the warming is limited in northwestern Europe owing to the intensified offshore high pressure and more northerly winds, while drier conditions prevail in the eastern Mediterranean, from the circulation around a relative heat low in northern Africa.

The frequencies of occurrence of the 5% drought in the 2020s and 2050s are shown in the upper left-hand corner of Plate 3 and Plate 4, respectively. In the 2020s, southern regions experience much greater frequency of drought,

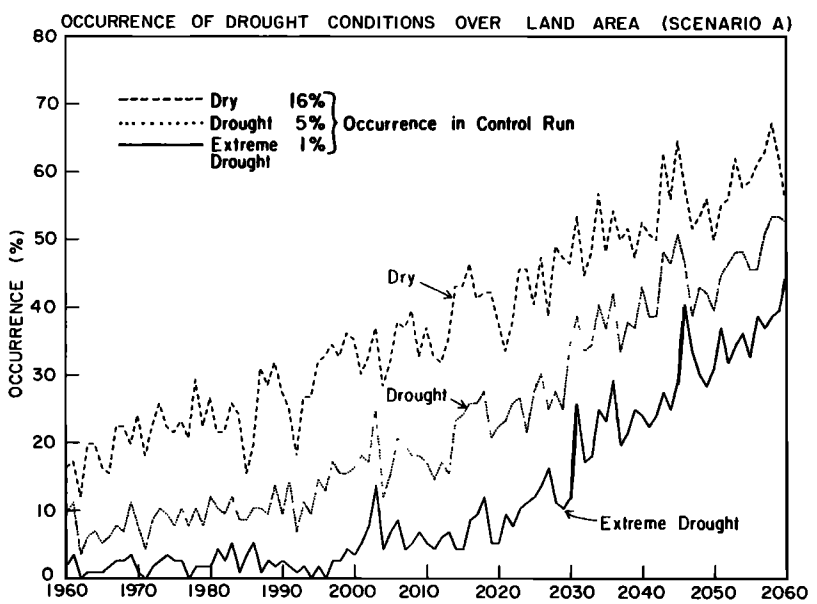

Fig. 2. Drought occurrence as a function of time during June–August generated from the SDDI, with results averaged over all grid boxes which are 90% land (except Antarctica) [from *Hansen et al.*, 1989].

TABLE 4. Seasonal Variation of SDDI Drought-Flood Categories

	<−1%	<−5%	<−16%	<−36%	>36%	>16%	>5%	>1%
				1990s				
Spring	1	7	22	40	32	17	7	2
Summer	1	7	19	38	37	18	8	1
Fall	1	6	21	44	31	13	6	1
Winter	2	7	16	44	33	14	6	1
Annual	1	7	20	42	33	15	7	1
				2020s				
Spring	8	17	40	67	16	6	3	1
Summer	7	14	32	61	17	6	2	0
Fall	6	16	43	67	16	7	1	0
Winter	5	20	45	69	15	7	2	0
Annual	7	17	40	66	16	7	2	0
				2050s				
Spring	38	52	68	80	10	5	1	0
Summer	21	38	63	80	9	2	1	0
Fall	31	56	73	85	8	2	1	0
Winter	32	53	68	83	10	4	1	0
Annual	30	50	68	82	9	3	1	0

All values are percentages.

although most of the country is affected. This is associated with the general northward progression of large E_P increases shown in Plate 1. By the 2050s, droughts occur in some regions 80% of the time as large E_P increases cover mid-latitudes (Plate 1).

To illustrate the method of calculation with the notation in equations (3)–(5), for the summer of the 2050s, we can use the control run and climate changes given in Table 1. For the current climate, $P - E_P = -30.4$, and for the 2050s, $P - E_P = -40.0$. Thus, $d_{SDDI} = -9.6$. With the standard deviation σ(equation (4)) = 15.8, $Z_{SDDI} = -0.53$. With this value of Z, the average change in index Y (equation (5)) was equal to −5.4.

It is important to note that these changes are driven primarily by the increased potential evapotranspiration associated with temperature changes, not by changes in precipitation. For example, the increase in the 5% drought in Alabama in all 3 decades is accompanied by little overall precipitation change, and as noted in Table 1, summer rainfall increases for the United States in the 2050s. Given the relative similarity in temperature projections among the different GCM groups, SDDI results should be more robust and reproducible from model to model than indices associated with hydrologic variables alone.

Results have been presented for summer, but drought in other seasons is a concern as well. As the monthly drought index is a function of the previous value, there is some continuity from season to season, although individual areas may differ. Table 4 gives the averages over the United States for the different drought-flood categories in the different seasons. By the 2050s, the drought values for summer are actually the least for any season, owing to the reduced warming and also somewhat greater precipitation increase during this time of year.

To summarize the results for the country as a whole, Figure 3 shows the variation of the annual average 1%, 5%, and 16% dry categories averaged over the United States, given as 5-year running means. Dry conditions (i.e., 16% occurrence in the control run) are experienced in a sustained fashion in the early 2000s. Drought conditions (5%) and extreme drought (1%) increase noticeably by that time but have their biggest jump near 2030. As can be seen from Plate 1, it is at this time that the large increases seen in the tropics and subtropics in earlier decades reach the United States on the average.

5.2. *PDSI Analysis: Transient Experiment*

The PDSI evaluates anomalous years within a climate regime. The "expected" values are derived from the full set of years under consideration, and the anomalous year stands out in contrast to these expectations. In this context, climatology (either observed or modeled) is used to generate the coefficients for the expected values, and the climate change results represent the anomalous years. In particular, it is important not to recalculate the coefficients for E_P as climate changes, to avoid underestimating E_P for the new climate.

Three different methods are used in applying model climate changes to the PDSI. The simplest procedure is to use real world climatology (from 1951 to 1980) to derive the Thornthwaite E_P parameters and the PDSI coefficients, and then apply the model-predicted changes to the observed temperature and precipitation values. This procedure is used for the doubled CO_2 results presented at the end of this section. As it uses the base climatology, it is referred to as the "base case" (PDSI-base, or PDSI-B).

Alternatively, the GCM values for the current climate can be used to generate the coefficients for the individual states. The climate change results are then used with these control run coefficients, which differ from the real world values on account of the difference in the model's temperature and (especially) precipitation values from observations. As this approach uses actual climate change estimates, it is referred to as "PDSI-actual" (PDSI-A).

In the third approach, the GCM values are modified. By comparison of the model and observed climatologies, a ratio is constructed indicating how far off the model's temperature and precipitation values are for each location. This ratio is then applied to the GCM temperature and precipitation, for both the control run and the climate change estimates. The

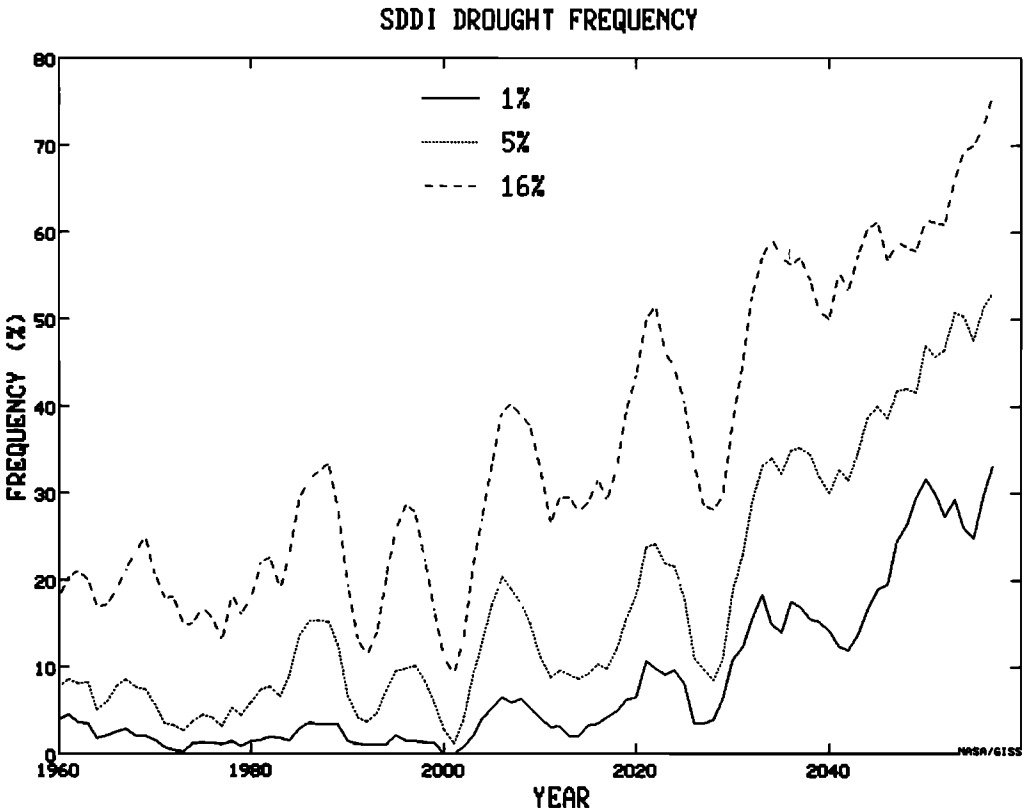

Fig. 3. As in Figure 2 except showing 5-year running (centered) mean annual-averaged values for the contiguous United States.

underlying assumption is that if the model produces twice as much rain as is observed, its precipitation changes will be 2 times too large. While this assumption may have some validity [*Rind*, 1988*b*], at the very least it is unlikely to be quantitatively accurate; furthermore, the temperature and precipitation changes are no longer self-consistent (since the corrective factor is generally different for the two quantities). Since this technique corrects model results through the use of ratios, it is referred to as "PDSI-ratio" or (PDSI-R).

The indices that are exceeded to produce the different categories of drought and flood are given in Table 3, and these are then used to define the future drought categories. (Note that 5% drought corresponds to a PDSI value close to −4, the value that represents the beginning of "extreme drought" in PDSI characterizations).

The results for the actual and ratio methods are shown as the top right and bottom left images in Plates 2–4 for the 1990s, 2020s, and 2050s. There are obviously many similarities in the changes shown by all three indices; in magnitude, the PDSI-actual, and PDSI-ratio values seem to bracket the SDDI. In the west, the PDSI-ratio method shows greater drought tendencies than does PDSI-actual. With the ratio method, the temperature changes are not altered greatly, since the GCM reproduces observed temperatures fairly well; however, the precipitation changes are altered significantly, being reduced in the west where the model has too much rain for the current climate. The precipitation changes thus become less effective in the west relative to temperature in the PDSI-ratio, and larger drought increases are indicated there.

The sensitivity of the PDSI to temperature and precipitation changes is explored further in Table 5, which gives the percentage occurrence of states in each drought-flood category for specified changes to the climatological data. For example, a 4.4°C change in temperature (close to the doubled CO_2 climate change over the United States) increases the mean PDSI to −5.6 and the 1% drought category in the climatology to 48%. To bring the mean PDSI back to 0 requires a 30% precipitation increase over the United States. The small precipitation change for the United States predicted by the GISS GCM for doubled CO_2 (of 6.33%) is completely dominated by the temperature effect, as is shown in the table.

A comparison of the changes forecast by the different indices and techniques for the full range of droughts and floods is presented in Table 6 for the summers of the 1990s, 2020s, and 2050s. The PDSI-ratio shows a slightly higher frequency of the most extreme droughts, while the SDDI has slightly more negative values overall. Nevertheless, the three indices produce relatively similar results.

We illustrate the PDSI-actual changes for summer of the 2050s using the results shown in Table 1, and the average values of the coefficients. Using equation (10), and substituting in the values appropriate for the United States as a whole, we get

$$\begin{aligned} d_{\mathrm{PDSI}} &= P - (\alpha\, E_P + \beta\ \mathrm{PR} + \gamma\ \mathrm{PRO} - \delta\ \mathrm{PL}) \\ &= 4.22 - (0.88 * 5.83 + 0.04 * 1.87 \\ &\quad + 0.09 * 6.10 - 0.27 * 3.90) \\ &= -0.48 \end{aligned} \tag{13}$$

TABLE 5. PDSI Sensitivity Tests Averaged Over the United States in Summer

Climatic Change	<−1%	<−5%	<−16%	<−36%	>36%	>16%	>5%	>1%	Mean PDSI
+1°F (0.55°C)	2	8	24	45	29	12	3	0.5	−0.6
+2°F (1.1°C)	4	13	33	54	23	8	2	0.3	−1.2
+4°F (2.2°C)	11	30	55	73	13	4	1	0.1	−2.5
+8°F (4.4°C)	48	72	87	93	3	1	0.1	0	−5.6
+8°F, +6.3%*P*	32	56	76	87	6	2	0.3	0	−4.4
+8°F, +20%*P*	12	27	45	61	23	11	4	0.7	−1.8
+8°F, +30%*P*	5	14	27	43	40	24	12	5	0.0
+8°F, +40%*P*	3	7	16	29	58	44	28	15	1.3
+8°F, +50%*P*	1	4	10	19	72	61	48	32	2.9

P indicates precipitation.

Then, from (11) we obtain the moisture anomaly

$$Z_{\mathrm{PDSI}} = kd$$

$$= 1.44 * (-0.48)$$

$$= -0.69$$

This mean moisture anomaly produces an average change of −2.2 for the PDSI-actual in summer. Note that the moisture anomaly Z_{PDSI} is similar in magnitude to Z_{SDDI} because of the normalizations used, despite the fact that the E_P values are very different. Differences in average value of the two indices may arise because the PDSI has a "backtracking" feature which does not appear in the SDDI. As shown by the example given in Table 2, both the PDSI and the SDDI require the same increase in $(P - E_P)/\sigma$ for 1 month to return their index to zero. However, the PDSI is also reset to zero whenever a "percentage probability" that an established drought or wet spell has ended is exceeded [*Palmer*, 1965] (usually accomplished by having several wet or dry months in a row). As the SDDI does not have this "automatic return" feature, it is consistently driven to higher values by the continued warming.

The 5-year running mean PDSI drought percentages for the United States as a whole are presented for the actual and ratio methods in Figures 4 and 5. Comparison with the SDDI in Figure 3 shows that the three indices have the same general track with time but on the annual average, the SDDI reaches somewhat higher values due to the absence of the backtracing feature.

5.3. *PDSI Analysis: Doubled CO_2*

Finally, we applied the PDSI analysis to the doubled CO_2 changes produced in the GISS model [*Hansen et al.*, 1984] and for comparison, to the results from the GFDL model [*Manabe and Wetherald*, 1987] as well. Ten-year averages were used from the equilibrium doubled CO_2 results in each case. As was noted previously, the technique involved altering the historical monthly values for each state from 1951 through 1980, which means that the variability being used for the doubled CO_2 climate is the same as the current variability, rather than that inherent in either the GISS or GFDL GCMs. *Rind et al.* [1989] show that the modeled hydrologic variability increases in general in the warmer climate, while temperature variability decreases, and these changes, of the order of 10%, are probably amplifying the previous results somewhat.

The results for the 5% drought (using the PDSI-B criteria presented in Table 3) are shown in Plate 5. Both models indicate a large increase in drought frequency, but the GFDL results are more extreme than the GISS doubled CO_2 results because the GFDL simulation produces warmer tempera-

TABLE 6. Variation of Drought-Flood Percentages During Summer

	<−1%	<−5%	<−16%	<−36%	>36%	>16%	>5%	>1%
				1990s				
SDDI	0.7	7	19	38	37	18	8	0.7
PDSI-ratio	2	8	20	41	37	22	7	0.7
PDSI-actual	0.4	7	17	37	39	25	8	2
				2020s				
SDDI	7	14	32	61	17	6	2	0.2
PDSI-ratio	8	16	29	49	28	9	2	0.2
PDSI-actual	4	10	25	44	33	15	6	1
				2050s				
SDDI	21	39	63	80	9	2	1	0.3
PDSI-ratio	22	41	58	74	13	5	1	0.2
PDSI-actual	10	26	52	67	16	6	2	0.6
				Doubled CO_2				
PDSI-B GISS	31	51	71	82	11	5	1	0.3
PDSI-B GFDL	67	83	93	98	1	1	0.5	0.3

All values are percentages.

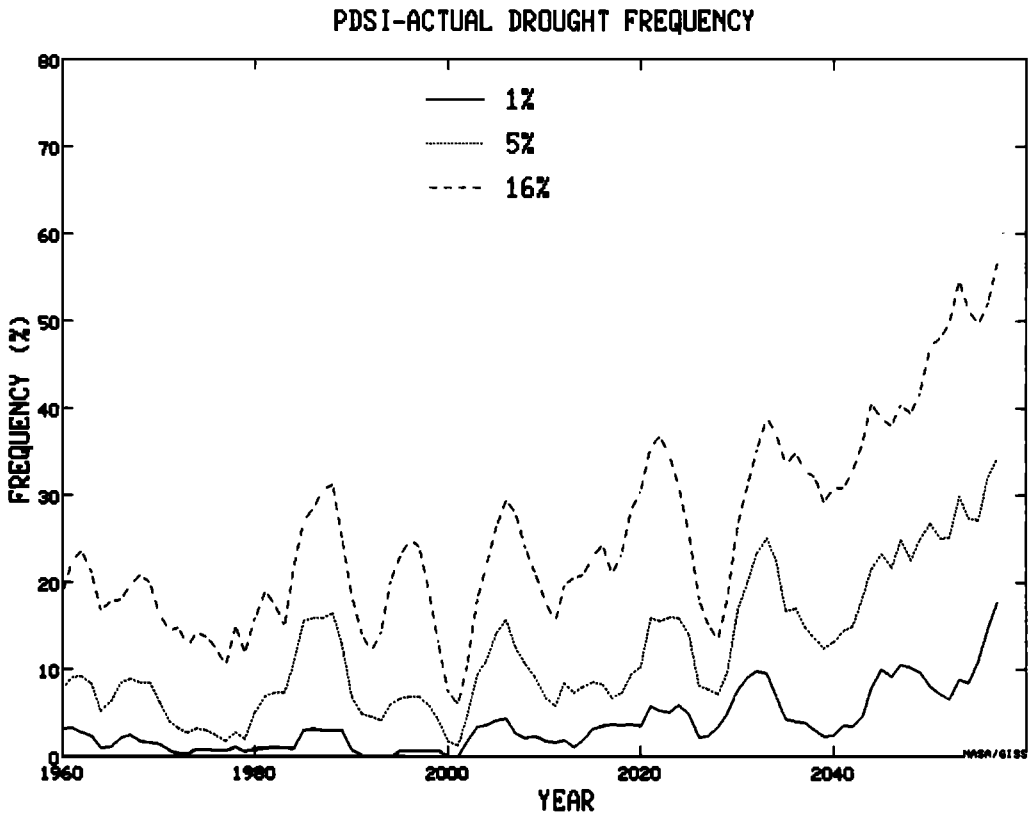

Fig. 4. As in Figure 2 using the PDSI-actual data.

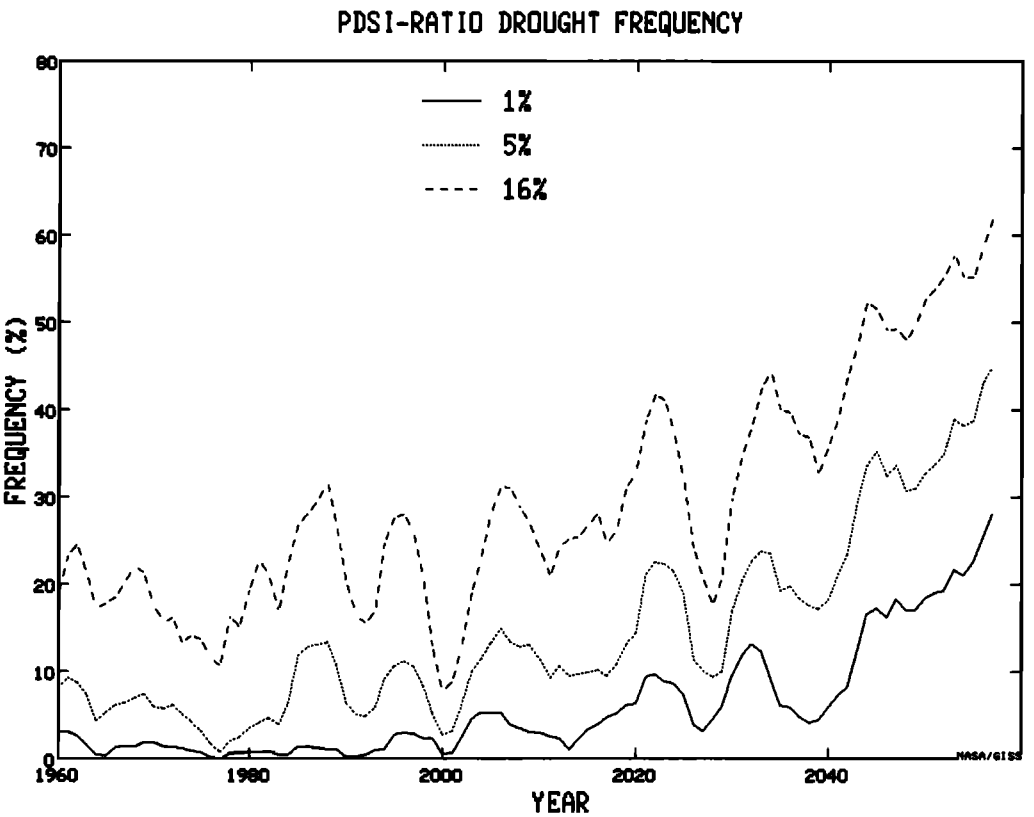

Fig. 5. As in Figure 2 using the PDSI-ratio data.

tures and less rainfall in summer relative to its control run than the changes that occurred in the GISS doubled CO_2 experiment. This result emphasizes that the GISS GCM climate warming projections are not overly extreme within the context of other modeling groups. As is shown in Table 5, the average PDSI change over the U.S. in the doubled CO_2 summer (4.4°C increase, 6.33% precipitation increase) is −4.4, which in PDSI terminology gives extreme drought as the average condition.

The percentage occurrences in the different doubled CO_2 drought categories are shown in Table 6. The difference between the PDSI value for the GISS doubled CO_2 and the value for the 2050s is due primarily to the aforementioned "backtracking feature," which comes into play more often with the variability inherent in the transient experiment results than with the average doubled CO_2 changes appended onto each of the base case months. The method used for the doubled CO_2 analysis applied an average change to the observed data, which in effect meant that every month was made warmer. The backtracking-resetting feature was thus minimized. With the actual model variability, drought was terminated more often, and the drought index did not build to as large values.

6. Discussion

6.1. *Likelihood of Future Drought*

Both drought indices show increased likelihood of drought as the climate warms, and for the latter half of the next century they indicate that the 5% drought occurs the majority of the time. The forecast therefore does not depend on the exact definition of the drought index employed, nor on a specific method of calculating E_P. Nevertheless, given the uncertainties in climate projections, how much confidence can we place in these results?

Both drought indices are dominated by the change in E_P due to the warmer climate, explicitly in the SDDI and implicitly in the PDSI with its E_P changes efficiently converted into evaporation increases. The results therefore depend on the magnitude of the climate warming, as well as its timing. In the doubled CO_2 experiments, both the GISS and GFDL models produce ~4°C global average warming, and if the true climate sensitivity is somewhat different, the drought occurrence will be modified accordingly. The treatment of clouds is especially important in this regard and will also affect local ground temperature and E_P results. In the transient experiment the results shown here are from scenario A, in which trace gases continue to increase exponentially. If the rate of future trace gas growth is slower, then the increase in drought frequency also will be slower.

The increase of drought in the tropics is heavily dependent upon the magnitude of the tropical warming. Currently, models differ on the amount of warming to be expected at low latitudes; for example, the GFDL model produces considerably less tropical warming than the GISS model [e.g., *Rind*, 1987]. The true climate sensitivity in this area is especially uncertain.

The SDDI indicates extreme drought in the 2050s and doubled CO_2 climate, despite the fact that the GISS hydrologic balance shows little change in soil moisture (Table 1). This is because the small value of β in the model prevents the E_P increase from being effectively translated into increased ET; carried to an extreme if β were to approach zero, even infinite temperature increases would not produce large increases in evaporation. This is the case of alternative A in section 3.

Were the model to have a more realistic ground hydrology scheme, it is possible that it would produce more evaporation, which might lead to more precipitation than is currently estimated, or, by reducing the soil moisture, result in even less precipitation over land. On a global basis, four GCMs run for doubled CO_2 all produce global precipitation increases in the range 9–15% [*Grotch*, 1989], which is much less than the 33% increase in atmospheric water-holding capacity that results from the 4°C warming. However, as none of these models has realistic land surface parameterizations, the possibility exists that they all produce unrealistic precipitation responses over land.

The same comment applies to the PDSI calculations. Here E_P changes are effectively converted to evaporation changes, so the Palmer balance gives a much larger increase in evaporation than is the case in the GCM. The Palmer hydrologic balance is indicative of alternative B described in section 3. The large evaporation increase leads to a soil moisture decrease of some 15% in the 2050s for the United States as a whole, and much larger decreases for certain states (Plate 4), while runoff in the 2050s decreases by 30% (Table 1) (similar to the results presented by *Revelle and Waggoner* [1983] in their empirical sensitivity studies of the effects of doubled CO_2 temperature on runoff). For the doubled CO_2 climate with the GISS model, the PDSI summer soil moisture decrease for the United States is 27%. However, the PDSI utilizes the temperature and precipitation changes generated by the GISS model. As is indicated in Table 5, if the warming were accompanied by a 30% increase in precipitation, the mean PDSI would return to 0. Note, though, that even in this case extremes still increase; even with the current land surface model, the GISS GCM produces greater hydrologic variability in the warmer climate [*Rind et al.*, 1989].

We can estimate in a crude fashion how the low β values in the GCM influence the climate change results by comparing the doubled CO_2 changes over a surface with a high value of β, the oceans (with $\beta = 1$), to those over land. Precipitation increases over land were actually larger than over the ocean by a factor of 2, implying that the forecast of increasing drought is not strongly dependent on the low change of β. The global precipitation change is controlled by the change in evaporation from the ocean. In the doubled CO_2 equilibrium, over land $\Delta T_G = 4.5$°C, and $\Delta T_S = 4.48$°C, so the saturated value of $Q_G - Q_S$ increases by some 40%. In contrast, over the oceans $\Delta T_G = 3.0$°C and $\Delta T_S = 3.2$°C, so the saturated value of $Q_G - Q_S$ increases by only 16%. The ocean increase would have been 30% if $T_G - T_S$ had remained constant, but the land surface warms more than the ocean (which readily responds to increased energy with fluxes of latent heat); the warmer air from the land then moves out over the ocean and reduces the lower level vertical temperature gradient (aided by the radiative effect of increased atmospheric opacity). E_P over the ocean is further reduced because the increase in low level stability reduces the drag coefficient (equation (1)). The land-ocean warming contrast limits the ability of the ocean evaporation and global precipitation ($\Delta P = 11\%$) to keep pace with the E_P increase over land. In the transient experiment the land-ocean warm-

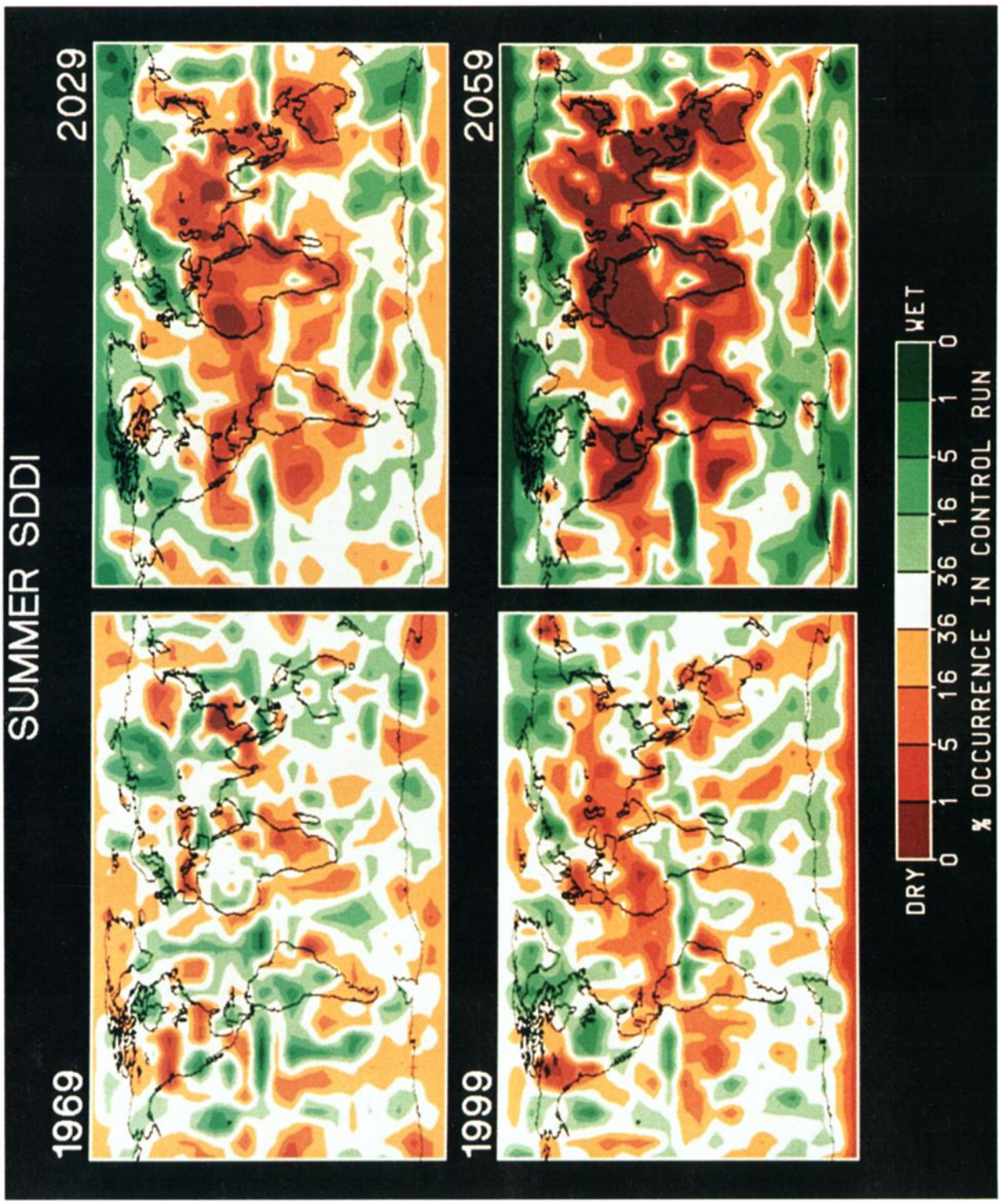

Plate 1. SDDI for June–August in the GISS global climate model simulation for trace gas scenario A. The color scale is set by the frequency of occurrence of a given drought index in the 100-year control run which had 1958 atmospheric composition. Results are shown for 1969, 1999, 2029, and 2059.

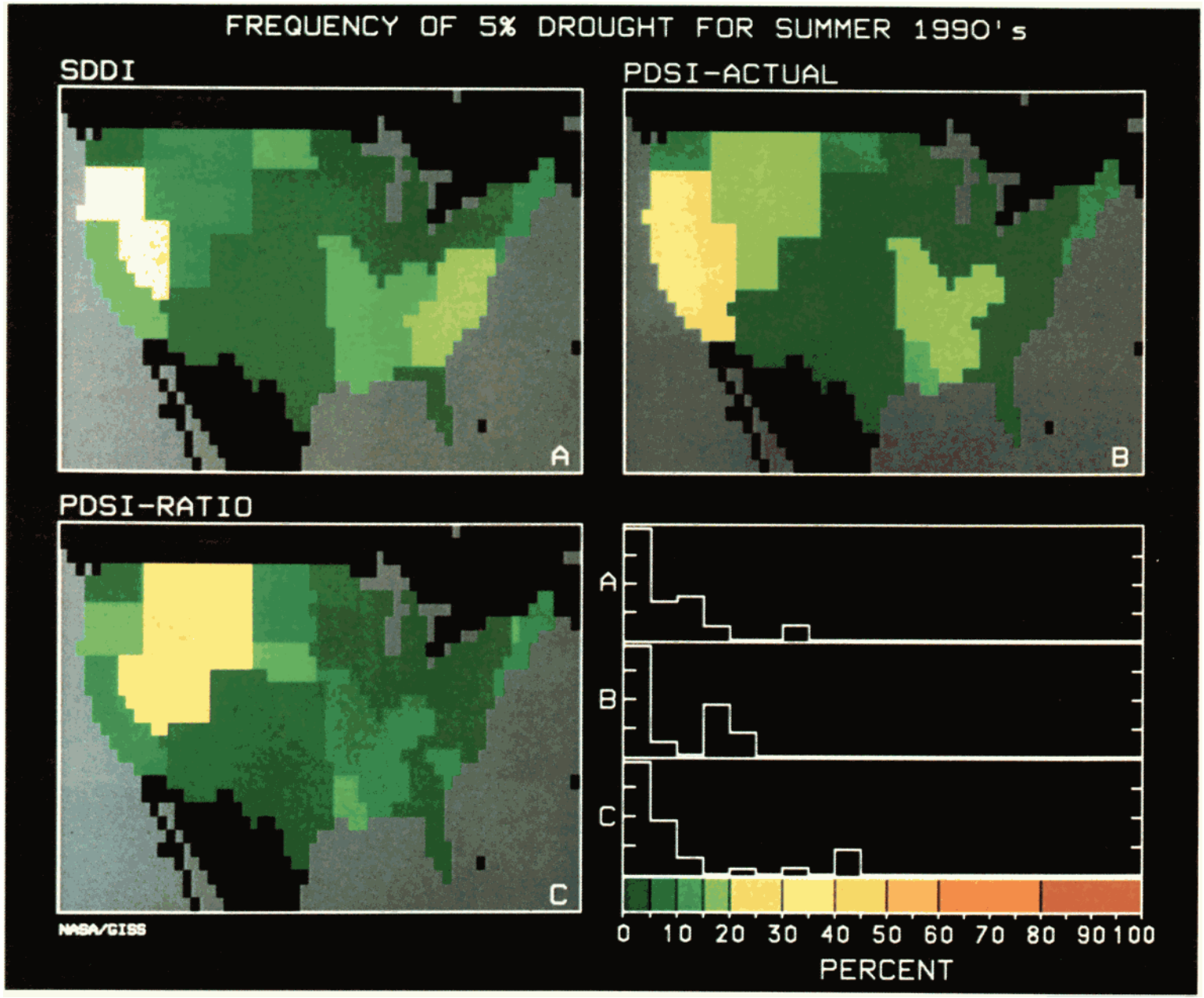

Plate 2. Frequency of occurrence of 5% drought values (in the control run) over the United States during summer for the 1990s for (*a*) SDDI, (*b*) PDSI-A, and (*c*) PDSI-R. The hodograph at bottom right gives the relative percentages in each category. Full scale represents 49%, 54%, and 50% for Plates 2*a*, 2*b*, and 2*c*, respectively.

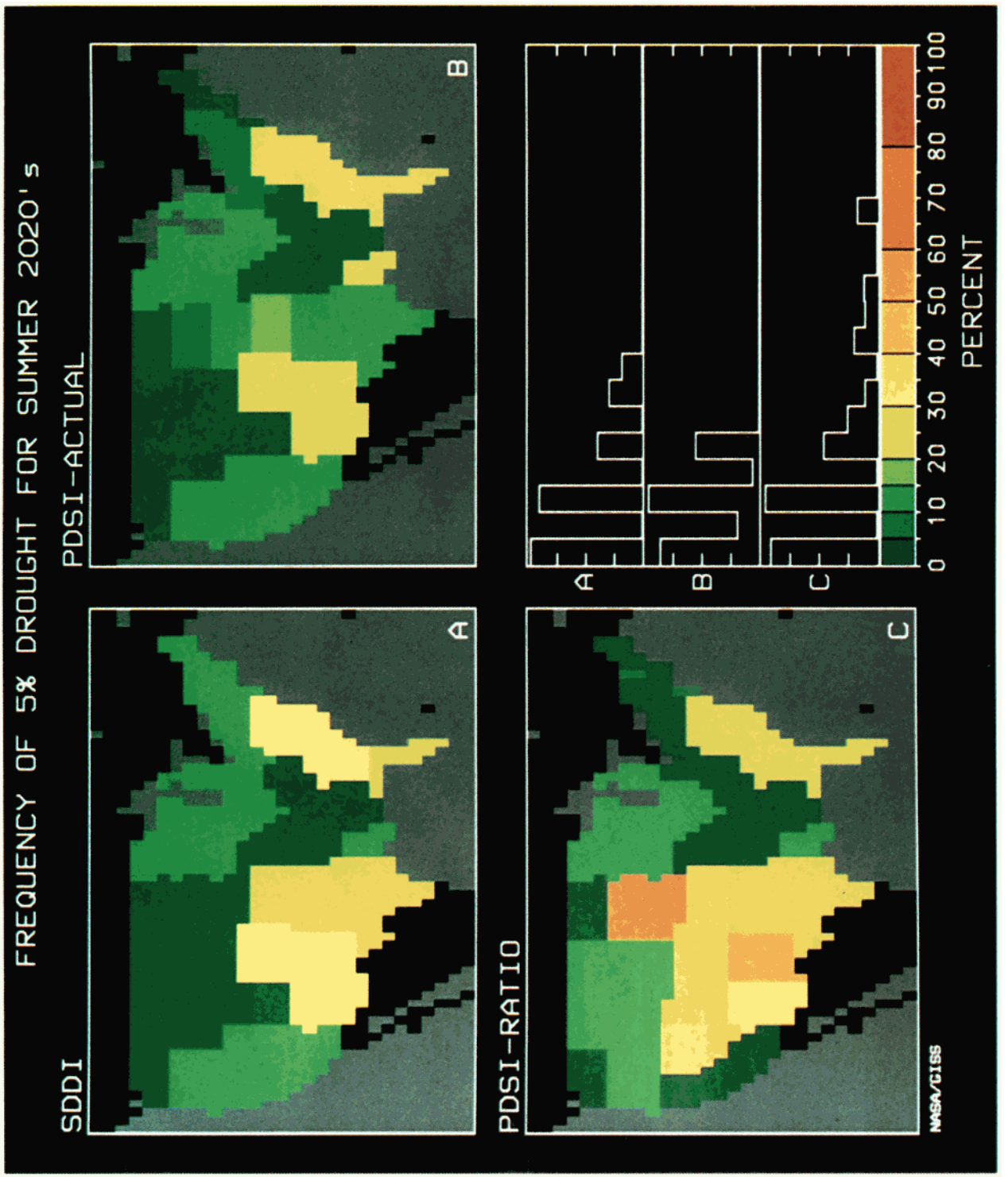

Plate 3. Frequency of occurrence of 5% drought values during summer as in Plate 2, for the 2020s. Full scale in the hodograph represents 35%, 36%, and 39% for Plates 3*a*, 3*b*, and 3*c*, respectively.

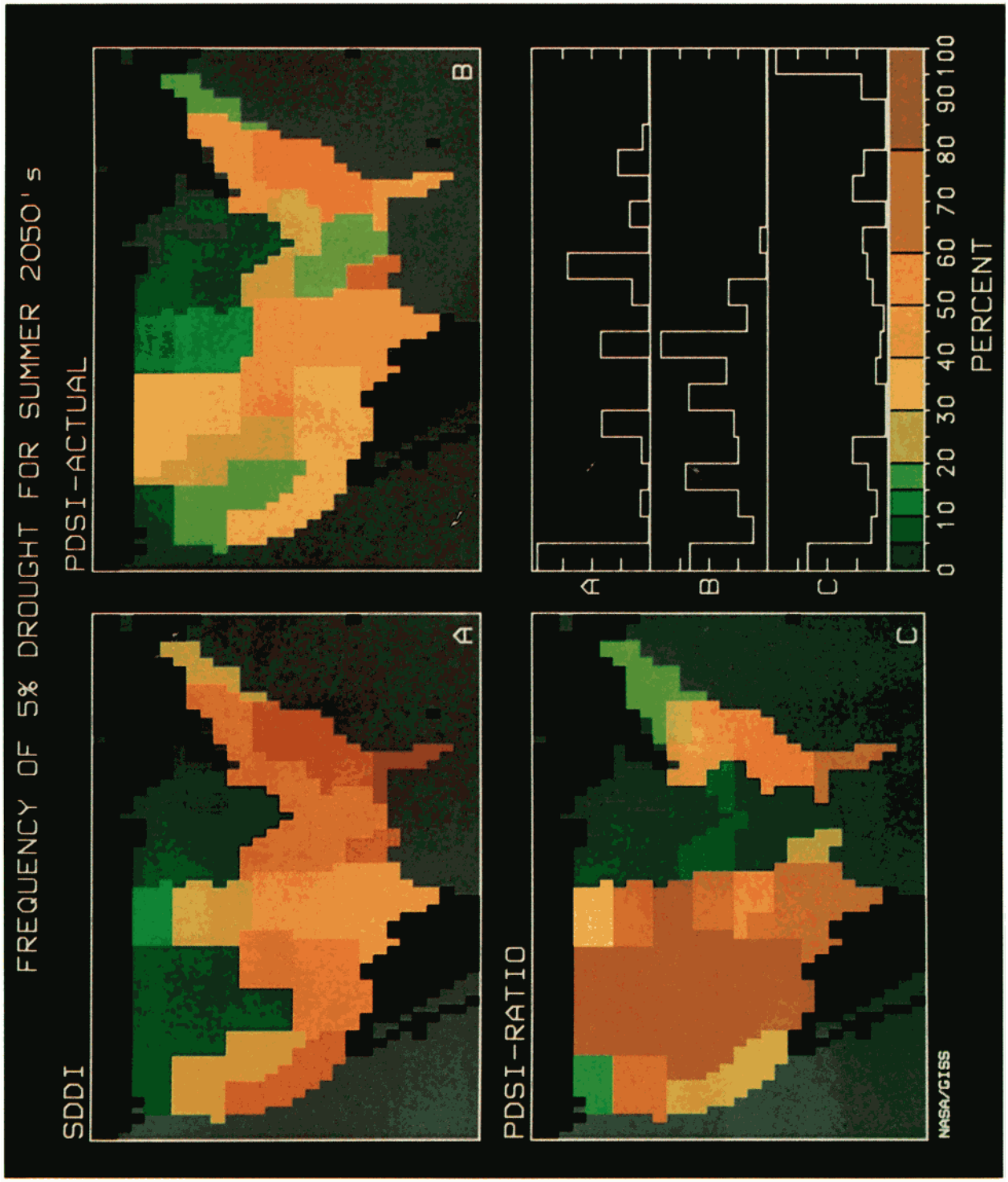

Plate 4. Frequency of occurrence of 5% drought during summer as in Plate 2, for the 2050s. Full scale in the hodograph represents 29%, 19%, and 25% for Plates 4*a*, 4*b*, and 4*c*, respectively.

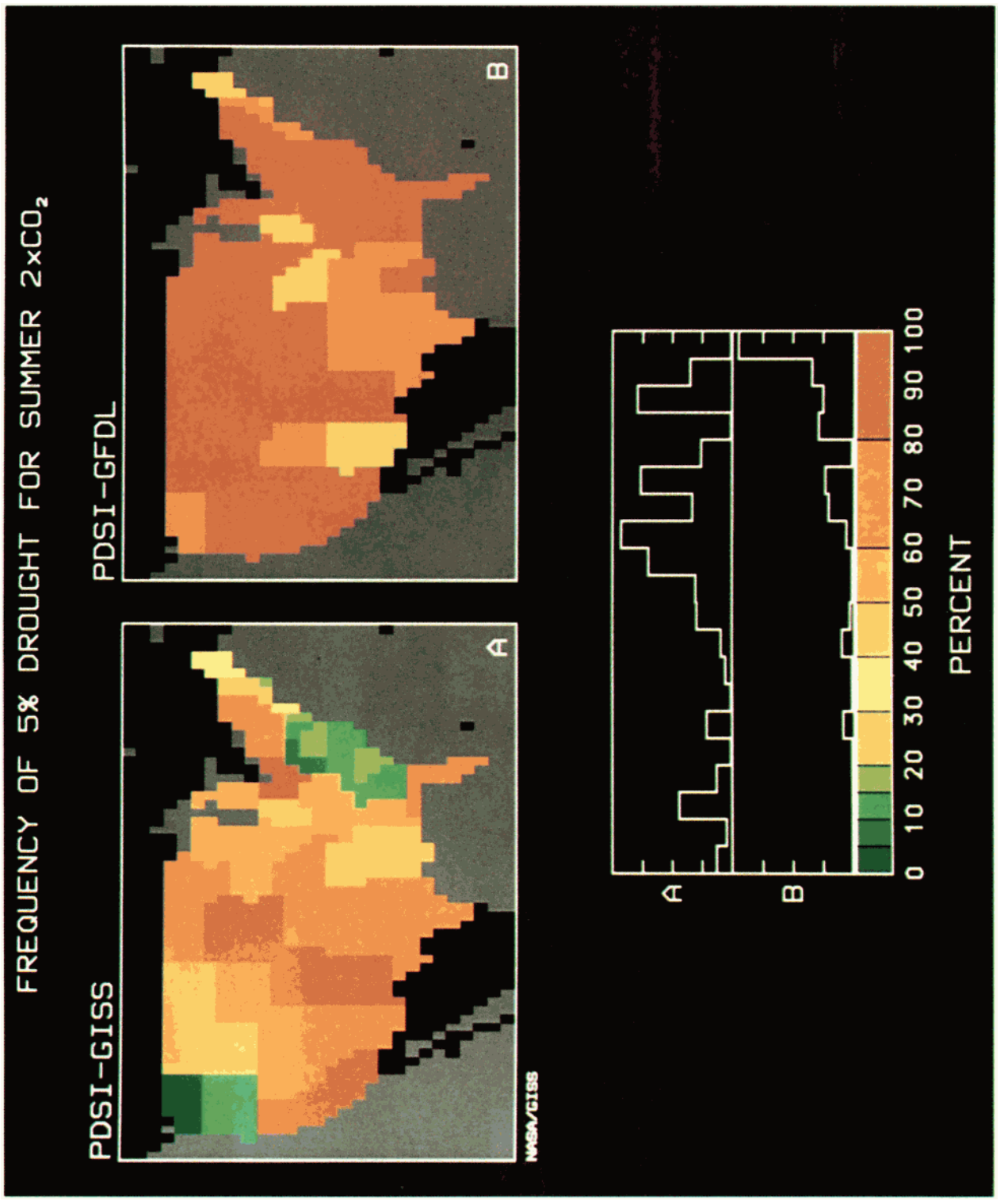

Plate 5. Frequency of occurrence of 5% drought during summer for (*a*) GISS doubled CO_2 results and (*b*) GFDL results using the PDSI-B. Full scale in the hodograph represents 16% in Plate 5*a* and 37% in Plate 5*b*.

ing contrast is even greater by 2060 owing to the longer ocean response time, so $\Delta P = 9.5\%$.

The drought indices emphasize an imbalance driven by the Clausius-Clapeyron relationship. As the summer warming is relatively uniform, the E_P increase is greatest where air is already warmest (i.e., low to middle latitudes), where the greatest absolute change in moisure-holding capacity occurs. The general precipitation increase occurs where the absolute moisture increase needed to achieve saturation is least, at higher latitudes where the temperature is coolest. For example, a warming of 5°C will increase the moisture-holding capacity of tropical surface air (at 25°C) by ~ 2.8 g kg^{-1}, while a similar warming at high latitudes (at 0°C) provides an increase of ~ 0.7 g kg^{-1}. With only one third of the needed moisture supplied in the tropics (as in the example given above), when transported to higher latitudes this is sufficient to saturate. The disparity in locations of increasing atmospheric demand (E_P) versus increasing supply (P) produces the results shown in Plate 1.

To prevent E_P from increasing in the warmer climate, the tropical relative humidity would have to increase by some 10% (using typical values from (1)). This is not likely from the standpoint of local dynamics because convection, which tends to dry the environment, should increase. It would be possible if poleward moisture transport were to decrease significantly. This depends on low latitude dynamics (i.e., Hadley cell), which acts to transport energy away from the tropics. An increase in tropical relative (and absolute) humidity would reduce outgoing longwave radiation, making it harder for the tropics to cool, and intensifying the need for poleward transports. Consistent with this reasoning, the models do not find increased relative humidity in the tropics in the warmer climate and do indicate increased poleward moisture transport [e.g., *Rind*, 1986, 1987], which leads to supersaturation and rainfall increases at high latitudes.

The determination of which local areas will be impacted most severely depends on regional climate simulations in GCMs, which are generally thought to be unreliable. However, as was noted in the discussion of the results, the model shows some specific regional sensitivities which are associated with the lag in ocean warming during the transient climate change. This is a reasonable feature of the climate system, which could be altered only by some process that has not been included, such as change in ocean heat transports. Note that while different model simulations for doubled CO_2 have failed to show consistent regional changes, they have not had the benefit of this transient oceanic response, since the equilibrium results have given the oceans time to warm fully.

6.2. *The Vegetative Response to Increased E_P*

The GISS GCM and PDSI hydrologic responses are indicative of alternatives A and B, respectively, from section 3, both of which effectively assume no change in vegetation. Here we explore the possibility that alternative C may occur: a reduction in ET efficiency (β) as the vegetation is desiccated and/or replaced by more sparse vegetation. To quantify prospective vegetation changes, we have examined different models of vegetative response to the projected doubled CO_2 climate.

Overpeck and Bartlein [1989] used the doubled CO_2 climate changes generated by the GISS model in conjunction with a forest stand simulation model [*Shugart*, 1984; *Solomon*, 1986] to estimate changes in forest composition in the eastern United States. The vegetation was given 300 years to adjust to the different climate, so the results do not represent the transient response, although subtropical trees were not allowed to migrate into the southern regions. The tree biomass in the eastern United States simulated at 28 locations decreased by an average of 40%, responding to both increased temperature directly, and to temperature effects on the hydrologic cycle (through increased E_P).

Peart et al. [1989], *Ritchie et al.* [1989], and *Rosenzweig* [1989] used the CERES and SOYGRO crop models for wheat, corn, and soybeans to estimate the impact of the doubled CO_2 climate changes on yields for selected sites in the Great Lakes region, the southeast United States, and the southern Great Plains. The yield decreases averaged over the different regions amounted to about 30% for the three crops with the GISS doubled CO_2 climate changes. Again, the response was primarily a result of increased temperature; the GISS doubled CO_2 precipitation changes averaged over the United States are actually slightly positive. With the GFDL doubled CO_2 changes, in which United States precipitation decreases and temperature increases are large, the agricultural yields averaged a 50% reduction. For both forests and crops, growing conditions improve at higher latitudes, where crops are currently limited by short growing seasons and low temperatures (and where the SDDI shows reduced drought frequencies (Plate 1)).

These models may be underestimating the actual vegetative response as a result of their methods of calculating E_P. The forest model recalculates the Thornthwaite E_P coefficients for the doubled CO_2 climate, which reduces the E_P change by implicitly assuming a more adaptive vegetation type. With the altered coefficients, the E_P change for the United States is underestimated by 30% when compared with the Priestly-Taylor method [*Priestly and Taylor*, 1972] used in the crop models, which itself may underestimate E_P in advective conditions [*Rosenberg et al.*, 1983]. In studies of vegetative reaction to climate change, it is important to quantify E_P and its changes as precisely as possible.

A third approach to estimating possible vegetation changes is represented by the climate-vegetation classification schemes, which, as we noted earlier, have historically recognized the importance of E_P. We use two such schemes to look at the latitudinal average change in vegetation type implied by the GISS doubled CO_2 climate changes. Shown in Table 7 are the average values of temperature and precipitation over land from the GISS GCM for both the current and doubled CO_2 climate simulations along with E_P changes calculated from the Thornthwaite method (without recalculating the coefficients). Currently, E_P exceeds P only in the subtropics. In the doubled CO_2 climate, E_P exceeds P everywhere south of 35°N. In the Köppen classification scheme this implies a shift in vegetation at these latitudes to "dry climate vegetation" (deserts, steppes, and prairies). In the *Holdridge* [1947] classification scheme, on the latitudinal average, "moist forest" shifts to "dry forest" (e.g., subtropical rainforest to woodlands and grassland), and "dry forest" to "very dry forest."

The Holdridge scheme changes in vegetation types represent a decrease in net primary productivity (NPP, the net carbon incorporated into the biosphere after autotropic respiration has been accounted for) of some 30% and 70%

TABLE 7. Annual Average Values Over Land

Latitude	Current Climate			Doubled CO_2		
	T, °C	P, mm d^{-1}	E_P, mm d^{-1}	T, °C	P, mm d^{-1}	E_P, mm d^{-1}
4° N	24.4	5.2	4.0	28.1	5.7	5.8
12° N	25.0	4.1	4.0	28.9	4.6	5.9
20° N	24.4	2.5	3.9	28.9	2.8	5.6
27° N	19.3	2.2	3.1	23.6	2.5	4.5
35° N	10.3	2.5	1.7	14.8	2.8	2.8
43° N	7.5	2.3	1.2	11.8	2.5	2.1

per unit area, respectively, using the NPP estimates of *Fung et al.* [1987]. This reduction in carbon uptake would likely be associated with reduced values of β; it would also affect the global carbon cycle. To quantify this effect, the study needs to be done by considering individual geographic regions and the imperfections of the schemes.

The biomass and vegetation classification results presented above did not take into account the so-called "direct effect" of carbon dioxide. Increased concentrations of atmospheric CO_2 have been shown to allow plant stomata to remain partially closed and limit transpirative water loss; at the same time, photosynthetic rates may be enhanced, especially in species with the C3 photosynthetic pathway (see, for example, *Strain and Cure* [1985]). Stomatal closure would decrease transpirative efficiency (β), as in alternative C, without limiting vegetation function. While these effects have been demonstrated in experimental settings, their applicability outside of the enclosed systems in which they have been observed, for example, over wide geographical areas and long time periods, is currently being debated [*Körner*, 1990].

Furthermore, the impact of the increased temperature on the energy of the plants must still be addressed. The only mechanism the plant leaf has to remove energy that does not involve a temperature increase is through transpiration; if transpiration is decreased, the leaf temperature tends to increase, amplifying the leaf-to-air vapor pressure deficit. As was illustrated previously for the bare ground simulated by GCMs, this tends to increase E_P, the atmospheric demand for moisture, and nullify part of the effect of stomatal control [*Allen et al.*, 1985]. Additionally, increasing temperature is itself detrimental to the plant, affecting photosynthesis and phenological processes if temperature optima are exceeded [e.g., *Larcher*, 1980]. As plant transpiration departs further from the potential rate, it seems likely that plant growth will be further from optimal.

Whether increased E_P leads directly to soil moisture loss, vegetation desiccation, or a simultaneous occurrence of both, the long-term result (decades to millenia) will likely be the same. The 15–30% reduction in soil moisture for the United States as a whole projected by the Palmer hydrologic balance would likely result in severe vegetation desiccation; in the forest stand model referred to previously, a 15% decrease in precipitation resulted in equilibrium biomass decreases of 50% in some locations. Conversely, without the stabilizing effect of vegetation, runoff increases as the impact of raindrops on the bare soil surface causes impervious crusts to form, reducing infiltration and soil moisture. On the longer time scales, lack of biological activity would lead to decreased soil production and increased erosion, reducing soil depth and water holding capacity. The absence of vegetation also increases the surface albedo, which can stabilize the atmosphere and reduce rainfall [*Charney et al.*, 1977]. In the GISS GCM, both reduced field capacity and increased albedo have the ability to reduce rainfall totals significantly, especially at low latitudes and in the summer hemisphere [*Rind*, 1984].

Probably the most likely result of increased E_P in the short run will be to decrease the soil moisture more than occurs in the GISS GCM and to decrease β by reducing vegetation biomass more than occurs in the PDSI. Desertification would then proceed, to whatever degree, by an interaction between the two effects.

6.3. *Paleoclimate Analogues for Warmth and Drought*

If large E_P increases ultimately result in desertification, the process should be apparent in paleoclimate reconstructions. Do past climates which are known to have been warm show extreme desiccation or arid conditions? A characteristic feature of the global SDDI (Plate 1) is that as the climate warms, lower latitudes are affected first on account of their greater increase in moisture holding capacity. We might then expect past warm climates to show aridity in the tropics and, with further warming, to have that aridity extend poleward.

A prime candidate for investigation is the climate of the Mesozoic, which in general is believed to have been warmer than that of today, both at extratropical and tropical latitudes (from the lack of land ice, isotopic ocean evidence, flora distributions, etc.). As was discussed by *Frakes* [1979], the Triassic started out cool (but nevertheless, warmer than today), temperatures warmed through the late Jurassic, and cooled in the late Cretaceous. *Hallam* [1985] has summarized the available hydrologic evidence and presented the schematics shown in Figure 6. Dry conditions prevailed throughout the tropics and subtropics in the early Triassic, expanded to higher latitudes (at least in the northern hemisphere) by the late Jurassic, and retreated again in the late Cretaceous. Experiments by *Kutzbach and Gallimore* [1989] for the early Triassic showed global warming of 1.5°–4.5° compared with today, values that are admittedly very uncertain. Note that the latitudes of aridity covered in these time periods are approximately the same as those shown in 2029 and 2059 (Plate 1) when the global average temperature is 2°C and 4°C warmer than today. Furthermore, the Mesozoic

wet regions are confined to the highest latitudes, as in the SDDI projections. In the late Cretaceous the cooler climate featured a return to wetter tropical conditions. The Mesozoic is an intriguing analog because the possibility exists that it was warm in association with increased CO_2.

During the Paleogene (from 65 to 23 million years ago), as climate cooled, there was a constriction of aridity from paleolatitude limits of somewhat more than 45° in the Cretaceous to slightly less than 30°, in general [*Frakes*, 1979]. As expected, the warm humid conditions at high latitudes also retreated equatorward [*Frakes*, 1979]. Overall arid conditions were not nearly as widespread as at earlier, warmer times. Low latitudes were not apparently marked by widespread aridity, nor were they obviously warmer than today [*Frakes*, 1979].

Throughout the Tertiary, desertification appeared to arise in specific locations as the climate cooled. These include the Namib desert in Africa [*Coetzee*, 1980] and the Atacama desert in northern Chile [*Alpers and Brimhall*, 1988], as well as deserts in western North America [*Axelrod*, 1950]. In the first two cases, increased offshore upwelling of cold water, associated with development of the Antarctic ice sheet, is thought to have reduced precipitation, while in the last case, elevation of the Rocky Mountains could have produced a rain shadow effect. These situations emphasize that drought is the result of changes in precipitation minus E_P, and can be produced by either decreased precipitation or substantially warmer temperatures. Reduced tropical precipitation due to cooler tropical waters may have been a factor in ice age tropical aridity. If warming locations remain humid (i.e., high relative humidity), E_P will not increase substantially. The SDDI, which includes precipitation, temperature, and humidity in its calculation, is thus an attempt to weigh all the relevant factors.

It may be that the deserts we find today are "climax" deserts, which have arisen at least partly from vegetation desiccation. The consequent albedo increases could have generated dynamic patterns of subsidence in response, as may be occurring today in the Sahel owing to direct anthropogenic effects. If some deserts are originally driven by vegetation desiccation, this may explain why GCM studies, which do not include vegetation feedback, do not seem to find the shifts in Hadley cell patterns of descent implied by paleodata; for example, subsidence patterns do not seem to arise spontaneously over the wide latitude range for aridity indicated in Figure 6 for Mesozoic simulations [*Rind*, 1986]. In general, the Hadley cell descent region does not appear to change markedly with climate forcing because of the many feedbacks inherent in the system [*Rind*, 1986]. Even the ice age studies fail to show the reported tropical drying [*Rind and Peteet*, 1985], perhaps because the vegetation was first reduced by cooler temperatures, again an effect not included in GCMs.

7. Concluding Remarks

The SDDI, which relates the change in the atmospheric supply and demand for moisture, and the PDSI, which calculates an independent water budget, both show a large increase in future drought over the United States due to warming associated with trace gas increases. The resultant increase in E_P may lead directly to soil moisture loss or to vegetation desiccation, but in either case a change to drier, sparser landscapes and biomes would result.

The review of soil moisture changes produced in five different GCMs run for doubled CO_2 [*Kellogg and Zhao*, 1988] indicated that three of the five produced soil moisture decreases for the United States during summer. Only the National Center for Atmospheric Research (NCAR) and GISS models failed to produce drying over most of the country. The NCAR results depend heavily on the fact that the control run is so dry that most of the additional spring rain in the warmer climate is retained by the model; in addition, NCAR summer soil moisture values in the control run are close to zero in some regions, so no reduction is possible [*Meehl and Washington*, 1988]. The results presented here suggest that the failure of the GISS model to show extensive soil moisture reduction is due to the unrealistic simulation of the land surface (i.e., the β value is very low), so the large E_P increases are not translated into evaporation increases. The possibility thus exists that all five of the GCMs would produce soil moisture decreases over the United States if these deficiencies were corrected. To the extent that all these models use similar E_P and ET parameterizations, soil moisture decreases may be underestimated in the models generally.

The full impact of the large E_P increases should become more apparent when GCMs incorporate more realistic ground hydrology models, including an active vegetation canopy [*e.g., Dickinson*, 1984; *Sellers et al.*, 1986; *Abramopoulos et al.*, 1988]. In effect, the vegetation would represent a thin, wet land surface in contrast with the thicker, partly wet land surface currently included in GCMs. This would allow for more accurate calculations of E_P changes, whose effect over vegetated surfaces could then be followed, especially if we include diagnostics indicative of the health of the vegetation. If the models produce unrealistic precipitation changes on account of the lack of vegetation canopy, this too should become apparent. Ultimately, we need to allow the vegetation to respond to the climate change. Improved land surface models could take into account the direct effect of CO_2 on transpiration, to the extent that it is understood on the large scale. They could also include carbon budget models, as well as temperature effects on other plant processes.

The magnitude and timing of these results depend primarily on the projected warming. This in turn depends on the rate of trace gas increase, the rate of ocean heat uptake, and the sensitivity of the climate system; to the extent that these are uncertain, the projections of future drought must be also. Note that the arrival of the equivalent doubled CO_2 global warming occurs near 2060 with the trace gas scenario used, which is probably too rapid if chloroflourocarbon production is drastically scaled back. Similarly, the 4°C sensitivity for doubled CO_2 may prove to be an overestimate and ocean heat uptake to be underestimated. Even were this true, the warming envisioned here may eventually be realized anyway, as there is no guarantee that trace gases with greenhouse capacity will stop increasing at the doubled CO_2 equivalent.

If and when a 4°C warming comes to pass, the salient point is that the atmospheric water holding capacity will increase by some 30%. This increase in atmospheric moisture de-

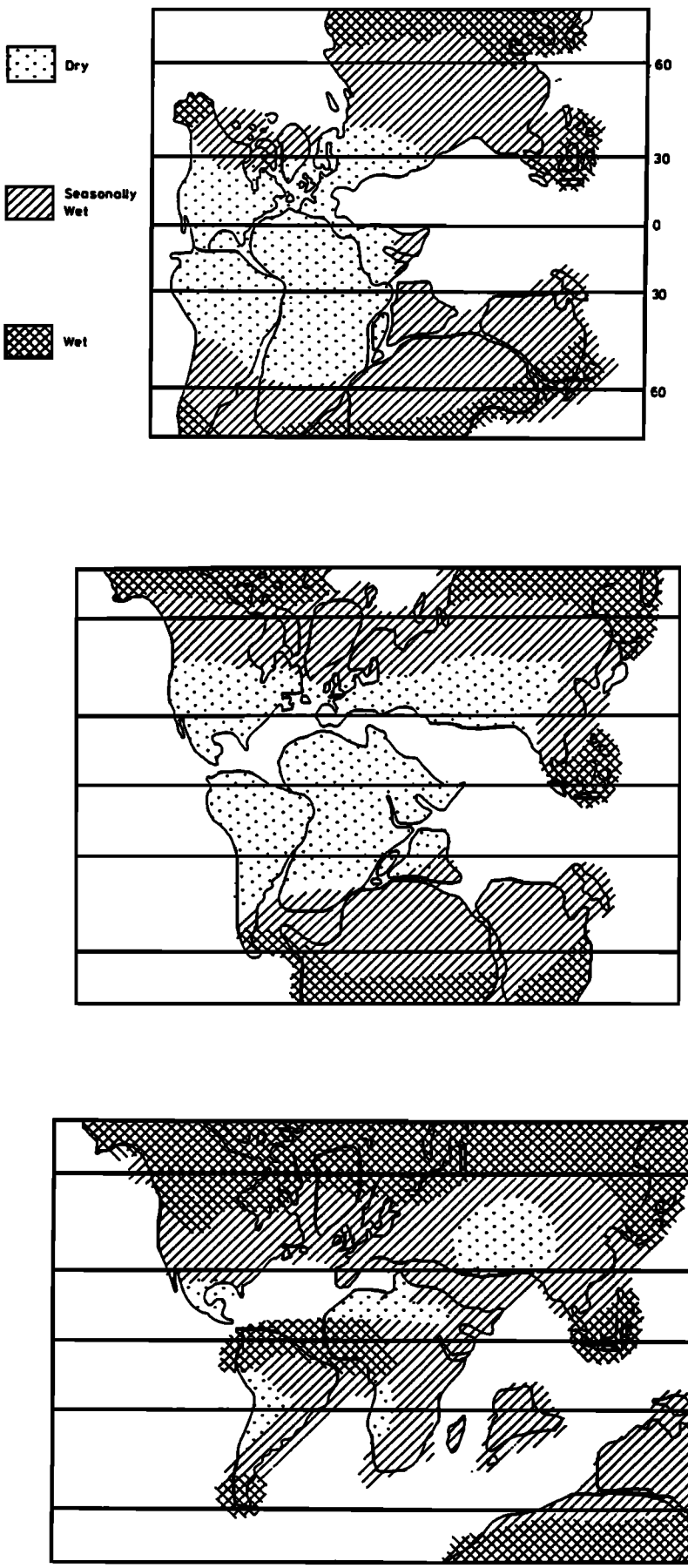

Fig. 6. Schematic presentation of continental humid and arid belts for (top) early Triassic, (middle) late Jurassic, and (bottom) late Cretaceous. (Reproduced by permission of the Geological Society from *Hallam* [1985].)

mand is translated to increased evapotranspiration with a very high efficiency over vegetation (under optimal growing conditions) and free water surfaces; it is thus similar in effect on available soil moisture to a 30% decrease in precipitation. The 30% reduction in runoff produced by the PDSI hydrologic budget and calculated from empirical studies is understandable in the light of these conditions. Because the precipitation increase is generally greatest at high latitudes while the increase in water-holding capacity is largest at lower latitudes, $P - E_P$ is bound to become more negative in many regions. On a global basis, the greater warming of the land surface guarantees that increases in ocean evaporation (and global precipitation) will be unable to keep up with the E_P increase over land.

If droughts of the severity indicated in this study come to pass, global habitability will be seriously affected.

Acknowledgments. We gratefully acknowledge useful discussions with Roger Anderson, Mark Chandler, Katie Prentice, Bill Ruddiman, and Daniel Hillel. We also thank Dick Wetherald and three anonymous reviewers for useful comments on the manuscript. Suke Manabe and Roy Jenne provided the GFDL doubled CO_2 data, and the National Climate Data Center provided the PDSI program and observational data. Patrice Palmer helped with the graphic displays. Modeling of greenhouse climate changes is supported by the United States Environmental Protection Agency offices of Policy Analysis and Research and Development, while our climate model development is supported by the NASA Climate Program Office.

REFERENCES

Abramopoulos, F., C. Rosenzweig, and B. Choudhury, Improved ground hydrology calculations for global climate models (GCMs): Soil water movement and evapotranspiration, *J. Clim.*, *1*, 921–941, 1988.

Allen, L. H., Jr., P. Jones, and J. Jones, Rising atmospheric CO_2 and evapotranspiration, in *Advances in Evapotranspiration*, pp. 13–27, American Society of Agricultural Engineers, St. Joseph, Mich., 1985.

Alley, W. M., The Palmer drought index: Limitations and assumptions, *J. Clim. Appl. Meteorol.*, *23*, 1100–1109, 1984.

Alpers, C. N., and G. H. Brimhall, Middle Miocene climatic change in the Atacama desert, northern Chile, *Geol. Soc. Am. Bull.*, *100*, 1640–1656, 1988.

Axelrod, D. I., Evolution of desert vegetation in western North America, in *Studies in Late Tertiary Paleobotany*, pp. 217–306, Carnegie Institute, Washington, D. C., 1950.

Baier, W., D. Z. Chaput, D. A. Russello, and W. R. Sharp, Soil moisture estimator program system, *Tech. Bull. 78*, 55 pp., Can. Dep. of Agric., Ottawa, 1972.

Carson, D. J., Current parameterization of land surface processes in atmospheric general circulation models, paper presented at JSC Study Conference on Land-Surface Processes in Atmospheric General Circulation Models, NASA, Greenbelt, Md., Jan. 5–10, 1981.

Charney, J., W. Quirk, S. Chow, and J. Kornfield, A comparative study of the effects of albedo change on drought in semi-arid regions, *J. Atmos. Sci.*, *34*, 1366–1385, 1977.

Coetzee, J. A., Tertiary environmental changes along the southwestern African coast, *Palaeontol. Afr.*, *23*, 197–203, 1980.

Deardorff, J. W., Empirical dependence of the eddy coefficient for heat upon stability above the lowest 50 m, *J. Appl. Meteorol.*, *6*, 631–643, 1967.

Delworth, T. L., and S. Manabe, The influence of potential evaporation on the variabilities of simulated soil wetness and climate, *J. Clim.*, *1*, 523–547. 1988.

Diaz, H. F., Drought in the United States: Some aspects of major dry and wet periods in the contiguous United States, 1895–1981, *J. Clim. Appl. Meteorol.*, *22*, 3–16, 1983.

Dickinson, R. E., Modeling evapotranspiration for three-dimensional global climate models, in *Climate Processes and Climate Sensitivity*, *Geophys. Monogr. Ser.*, vol. 29, *Maurice Ewing Ser.*, vol. 5, edited by J. E. Hansen and T. Takahashi, pp. 58–72, AGU, Washington, D. C., 1984.

Frakes, L. A., *Climate Throughout Geologic Time*, 310 pp., Elsevier, New York, 1979.

Fung, I. Y., C. J. Tucker, and K. C. Prentice, Application of advanced very high resolution radiometer vegetation index to study atmosphere-biosphere exchange of CO, *J. Geophys. Res.*, *92*, 2999–3015, 1987.

Gollan, T., J. B. Passioura, and R. Munns, Soil water status affects the stomatal conductance of fully turgid wheat and sunflower leaves, *Aust. J. Plant Physiol.*, *13*, 459–464, 1986.

Grotch, S. L., A statistical intercomparison of temperature and precipitation predicted by four general circulation models with historical data, paper presented at the DOE Workshop on Greenhouse-Gas-Induced Climate Change, U.S. Dep. of Energy, Univ. of Mass., Amherst, May 8–12, 1989.

Hallam, A., A review of Mesozoic climates, *J. Geol. Soc. London*, *142*, 433–445, 1985.

Hansen, J. G. Russell, D. Rind, P. Stone, A. Lacis, S. Lebedeff, R. Ruedy, and L. Travis, Efficient three-dimensional global models for climate studies: Models I and II, *Mon. Weather Rev.*, *111*, 609–662, 1983.

Hansen, J., A. Lacis, D. Rind, G. Russell, P. Stone, I. Fund, R. Ruedy, and J. Lerner, Climate sensitivity, analysis of feedback mechanisms, in *Climate Processes and Climate Sensitivity*, *Geophys. Monogr.* Ser., vol. 29, *Maurice Ewing Ser.*, vol. 5, edited by J. E. Hansen and T. Takahashi, pp. 130–163, AGU, Washington, D. C., 1984.

Hansen, J., I. Fung, A. Lacis, D. Rind, S. Lebedeff, R. Ruedy, and G. Russell, Global climate changes as forecast by Goddard Institute for Space Studies three-dimensional model, *J. Geophys. Res.*, *93*, 9341–9364, 1988.

Hansen, J., D. Rind, A. Delgenio, A. Lacis, S. Lebedeff, M. Prather, R. Ruedy, and T. Karl, Regional greenhouse climate effects, in *Preparing for Climate Change*, *Proceedings of the Second North American Conference on Preparing for Climate Change*, pp. 68–81, Climate Institute, Washington D. C., 1989.

Hecht, A. D., Drought in the Great Plains: History of societal response, *J. Clim. Appl. Meteorol.*, *22*, 51–56, 1983.

Hillel, D., *Soil and Water*, 288 pp., *Academic*, San Diego, Calif., 1971.

Hillel, D., *Introduction to Soil Physics*, 364 pp., Academic, San Diego, Calif., 1980.

Holdridge, L. R., Determination of world formulations from simple climatic data, *Science*, *105*, 367–368, 1947.

Karl, T. R., and A. J. Koscielny, Drought in the United States: 1895–1981, *J. Clim.*, *2*, 313–329, 1982.

Karl, T. R., and R. G. Quayle, The 1980 summer heat wave and drought in historical perspective, *Mon. Weather Rev.*, *109*, 2055–2072, 1981.

Karl, T. R., and W. E. Riebsame, The impact of decadal fluctuations in mean precipitation and temperature on runoff: A sensitivity study over the United States, *Clim. Change*, *15*, 423–448, 1989.

Kellogg, W. W., and Z.-C. Zhao, Sensitivity of soil moisture to doubling of carbon dioxide in climate model experiments, I, North America, *J. Clim.*, *1*, 348–366, 1988.

Köppen, W., Das geographische System der Klimate, in *Handbuch der Klimatologie*, edited by W. Koppen and R. Geiger, 46 pp., Borntraeger, Berlin, 1936.

Körner, C., CO_2 fertilization: the great uncertainty in future vegetation development, in *Global Vegetation Change*, edited by A. Solomon, D. Reidel, Hingham, Mass., in press, 1990.

Kramer, P. J., *Water Relations of Plants*, 489 pp., Academic, San Diego, Calif., 1983.

Kutzbach, J. E., and R. G. Gallimore, Pangaean climates: Megamonsoons of the megacontinent, *J. Geophys. Res.*, *94*, 3341–3357, 1989.

Langbein, W. B., Annual Runoff in the United States, *Surv. Circ. 5*, U.S. Dep. of the Inter., Washington, D. C., 1949.

Larcher, W., *Physiological Plant Ecology*, 303 pp., Springer-Verlag, New York, 1980.

Manabe, S., Climate and ocean circulation, I, The atmospheric circulation and the hydrology of the Earth's surface, *Mon. Weather Rev.*, *97*, 739–774, 1969.

Manabe, S., and R. Wetherald, Large-scale changes of soil wetness

induced by an increase in atmospheric carbon dioxide, *J. Atmos. Sci.*, *44*, 1211–1236, 1987.

Mather, J. R., Influence of predicted CO_2 increase on hydroclimatic factors, paper presented at the Fifth Conference on Applied Climatology, Am. Meteorol. Soc., Baltimore, Md., March 10–12, 1987.

Meehl, G. A., and W. M. Washington, A comparison of soil-moisture sensitivity in two global climate models, *J. Atmos. Sci.*, *45*, 1476–1492, 1988.

Overpeck, J., and Bartlein, P. J., Assessing the response of vegetation to future climate change: Ecological response surfaces, and paleoecological model validation, in *The Potential Effects of Global Climate Change on the United States*, Appendix D, *Forests*, edited by J. B. Smith and D. A. Tirpak, pp. 1-1–1-32, U.S. Environmental Protection Agency, Washington, D. C., 1990.

Palmer, W. C., Meteorological drought, *Res. Pap. 45*, U.S. Weather Bur., Washington, D. C., 1965. (Available from Libr. and Inf. Serv. Div., NOAA, Washington, D. C.).

Peart, R. M., J. W. Jones, R. B. Curry, K. Boote, and L. H. Allen, Impact of climate change on crop yield in the southeastern U. S. A., A simulation study, in *The Potential Effects of Global Climate Change on the United States*, Appendix C, vol. 1, *Agriculture*, edited by J. B. Smith and D. A. Tirpak, pp. 2-1–2-54, U.S. Environmental Protection Agency, Washington, D. C., 1990.

Penman, H. L., Natural evaporation from open water, bare soil, and grass, *Proc. R. Soc. A., London Ser.*, *193*, 102–122, 1948.

Prentice, K. C., Bioclimatic distribution of vegetation for general circulation model studies, *J. Geophys. Res.*, in press, 1990.

Priestley, C. H. B., and R. J. Taylor, On the assessment of surface heat flux and evaporation using large-scale parameters, *Mon. Weather Rev.*, *100*, 81–92, 1972.

Revelle, R., and P. E. Waggoner, Effects of a carbon dioxide induced climatic change on water supplies in the western U. S., in *Changing Climate*, pp. 419–432, National Research Council, National Academy Press, Washington, D. C., 1983.

Rind, D., The influence of vegetation on the hydrologic cycle in a global climate model, in *Climate Processes and Climate Sensitivity*, *Geophys. Monogr. Ser.*, vol. 29, *Maurice Ewing Ser.*, vol. 5, edited by J. E. Hansen and T. Takahashi, pp. 73–91, AGU, Washington, D. C., 1984.

Rind, D., The dynamics of warm and cold climate, *J. Atmos. Sci.*, *43*, 3–24, 1986.

Rind, D., The doubled CO_2 climate: Impact of the sea surface temperature gradient, *J. Atmos. Sci.*, *44*, 3235–3268, 1987.

Rind, D., The doubled CO_2 climate and the sensitivity of the modeled hydrologic cycle, *J. Geophys. Res.*, *93*, 5385–5412, 1988*a*.

Rind, D., Dependence of warm and cold climate depiction on climate model resolution, *J. Clim.*, *1*, 965–997, 1988*b*.

Rind, D., and D. Peteet, Terrestrial conditions at the last glacial maximum and CLIMAP sea-surface temperature estimates: Are they consistent?, *Quat. Res.*, *24*, 1–22, 1985.

Rind, D., R. Goldberg, and R. Ruedy, Change in climate variability in the 21st century, *Clim. Change*, *14*, 5–37, 1989.

Ritchie, J. T., B. D. Baer, and T. Y. Chou, Effect of global climate change on agriculture. Great Lakes region, in *The Potential Effects of Global Climate Change on the United States*, Appendix C, vol. 1, *Agriculture*, edited by J. B. Smith and D. A. Tirpak, pp. 1-1–1-20, U.S. Environmental Protection Agency, Washington, D. C., 1990.

Rosenberg, N. J., B. L. Blad, and S. B. Verma, *Microclimate, The Biological Environment*, 495 pp., John Wiley, New York, 1983.

Rosenthal, W. D., G. F. Arkin, and P. J. Shouse, Water deficit effects on sorghum transpiration, in *Advances in Evapotranspiration*, pp. 159–169, American Society of Agricultural Engineers, St. Joseph, Mich., 1985.

Rosenzweig, C., Potential effects of climate change on agricultural production in the Great Plains, A simulation study, in *The Potential Effects of Global Climate Change on the United States*, Appendix C, vol. 1, *Agriculture*, edited by J. B. Smith and D. A. Tirpak, pp. 3-1–3-43, U. S. Environmental Protection Agency, Washington, D. C., 1990.

Schlesinger, M. E., and J. F. B. Mitchell, Climate model simulations of the equilibrium climatic response to increasing carbon dioxide, *Rev. Geophys.*, *25*, 760–798, 1987.

Sellers, P. J., Y. Mintz, C. Sud, and A. Dalcher, A simple biosphere (SiB) for use within general circulation models, *J. Atmos. Sci.*, *43*, 505–531, 1986.

Shugart, H. H., *A Theory of Forest Dynamics*, 278 pp., Springer-Verlag, New York, 1984.

Shuttleworth, W. J., et al., Eddy correlation measurements of energy partition for Amazonian forest, *Q. J. R. Meteorol. Soc.*, *110*, 1143–1162, 1984.

Smith, J. B., and D. A. Tirpak (Eds.), *The Potential Effects of Global Climate Change on the United States*, 413 pp., U.S. Environmental Protection Agency, Washington, D. C., 1989.

Solomon, A. M., Transient response of forests to CO_2-induced climate change: Simulation modeling experiments in eastern North America, *Oecologia*, *68*, 567–579, 1986.

Stockton, C. W., and W. R. Boggess, *Geohydrological Implications of Climate Change on Water Resource Development*, U.S. Army Coastal Engineering Research Center, Fort Belvoir, Va., 1979.

Strain, B. R., and J. D. Cure, Direct effects of increasing carbon dioxide on vegetation, *Rep. DOE/ER-0238*, 286 pp., U.S. Dep. of Energy, Washington, D. C., 1985.

Sud, Y. C., and M. J. Fennessy, An observational-data based evapotranspiration function for general circulation models, *Atmos. Ocean*, *20*, 301–316, 1982.

Thornthwaite, C. W., An approach toward a rational classification of climate, *Geogr. Rev.*, *38*, 55–89, 1948.

Yao, A. Y., Agricultural climatology, in *World Survey of Climatology*, vol. 3, pp. 189–298, edited by H. E. Landsberg, 408 pp., Elsevier, New York, 1981.

Zhao, Z.-C., and W. W. Kellogg, Sensitivity of soil moisture to doubling of carbon dioxide in climate model experiments, II, The Asian monsoon region, *J. Clim.*, *1*, 367–378, 1988.

R. Goldberg and C. Rosenzweig, Center for the Study of Global Habitability, Columbia University, New York, NY 10027.

J. Hansen and D. Rind, Institute for Space Studies, NASA Goddard Space Flight Center, 2880 Broadway, New York, NY 10025.

R. Ruedy, Centel Sigma Data Services Corporation, New York, NY 10025.

(Received June 7, 1989;
revised December 14, 1989;
accepted December 21, 1989.)